Contrasting Trends in Colorado Fire Weather Index from Reanalysis and Observations

by

Max M. Silver

B.A. Statistics & Data Science, University of Colorado Boulder, 2023

A thesis submitted to the

Faculty of the Graduate School of the

University of Colorado in partial fulfillment

of the requirements for the degree of

Master of Science

Department of Applied Mathematics

2025

Committee Members:

William Kleiber, Chair

Julie K. Lundquist

Kristopher A. Pruitt

Silver, Max M. (M.S., Applied Mathematics)

Contrasting Trends in Colorado Fire Weather Index from Reanalysis and Observations

Thesis directed by Prof. William Kleiber

Recent wildfires in Colorado raise the question of whether rising global temperatures have increased fire weather occurrences in Colorado. The U.S. National Weather Service defines fire weather as when "forecast weather conditions will result in a significant threat for the ignition and/or spread of wildfires". We use two datasets to address the question: "How has the occurrence of fire weather changed in Colorado?" Using 22 years of observed weather conditions from a meteorological tower at the National Renewable Energy Laboratory and 67 years of ERA5 reanalysis data, we assess changing trends in Colorado fire weather occurrences. Additionally, we explore if the difference in recorded wind speeds between observational data and reanalysis data can be explained by differences in spatial and temporal resolution, and what are the implications in the context of quantifying fire weather occurrences. The observational data are limited in temporal extent and spatial representativeness, but they capture exact real-world conditions at a location in complex terrain. The reanalysis data are available for an extended period of time and for the entire state, but the data are of relatively coarse spatial and temporal resolution and may fail to capture extremes. To quantify fire risk, we calculate the Hot-Dry-Windy Index (HDWI), which relies on wind speed and vapor pressure deficit. No statistically significant trend in the HDWI appears in the observational dataset. However, according to the reanalysis data, strong increasing trends in HDWI values emerge across all of Colorado. This apparent conflict between observational and reanalysis data suggests that reanalysis data may not be representative and more long-term observational datasets are required to assess fire risk.

Contents

Chapter

Tables

Table

Figures

Figure

Chapter 1

Introduction

Wildfires in Colorado have posed several recent threats to life and property. In December 2021, the Marshall fire destroyed 1084 homes and 7 commercial buildings, and it damaged an additional 149 homes and 30 commercial buildings in Boulder County, Colorado (Flynn, 2022). Damages from the Marshall fire exceeded $2 billion (Brasch and Wertz, 2023). In 2020, the Cameron Peak fire burned almost 209,000 acres (Blumhardt, 2020), and the East Troublesome fire burned more than 190,000 acres (Gabbert, 2022) and caused almost $550,000 in damage (Phillips, 2022). Certain types of weather promote fire occurrences. The U.S. National Weather Service defines fire weather as where "forecast weather conditions will result in a significant threat for the ignition and/or spread of wildfires". These conditions include low relative humidity, strong surface winds, and warm temperatures; drought will also increase fuel availability. Understanding the prevalence and risk of fire weather occurrences may help develop mitigation and prevention strategies.

In the larger context of global climate change, fire weather occurrences are increasing globally as temperatures increase (Jain et al., 2022). Analysis of the annual 95th percentile for three parameters—the Canadian Fire Weather Index System's (CFWIS's) Fire Weather Index, the CFWIS Initial Spread Index, and the vapor pressure deficit (VPD)—between 1979 and 2000 found that each of the indices was significantly increasing in most regions of the world. Less than 3% of global burnable land mass showed a significant decrease in fire weather occurrences, and most of that land was in a tropical climate (Jain et al., 2022).

In the western United States, wildfire frequency and duration have also increased. Wildfire

season length is defined as the time (in days) between the first wildfire discovery in a year and the day the last fire of the year is controlled (controlling a wildfire happens after containment) (Westerling et al., 2006). Wildfire season length has increased since 1970, with the increase mostly coming during the 1980s (Westerling et al., 2006). This increase in season length arises from both earlier wildfire occurrences and later final wildfire control (Westerling et al., 2006). The delayed final control develops from both later fire ignitions and longer burning times. Balch et al. (2018) find that in the western United States, peak fire weather occurrences shifted to September starting in 2017, instead of in August between 2001 and 2016. The primary cause of this shift was a hotter and drier summer, which allows for more rapid fire spread.

Given this larger context of increasing fire risk due to climate change, a goal of this project was to quantify if and how much fire weather occurrences are increasing in Colorado in particular. Colorado's population is one of the fastest growing populations in the United States, and it is important to understand how fire weather are changing and how that will affect those living in Colorado (US Census, 2023). Accurate predictions of future fire weather occurrences can aid implementation of fire mitigation strategies, such as fire bans and fire restrictions. With growing concerns about rising temperatures due to global warming, it is important to understand how fire weather occurrences are changing as a result and which datasets can help us understand those patterns.

Here, we focus on changes in Colorado's fire weather occurrences over time to understand the role of climate change in fire weather occurrences. While several fire weather indices exist, we choose the Hot-Dry-Windy index (HDWI) (Srock et al., 2018). The HDWI is most suitable for determining days where weather conditions would contribute to a devastating fire. It does not consider ground moisture or topography, or their interactions with atmospheric conditions (Worsnop et al., 2021). Despite its streamlined inputs, the HDWI performs equally compared to other indices (Sharples, 2022), and so the HDWI is a useful measurement when data are limited. Worsnop et al. (2021) used the HDWI to predict future fire weather occurrences. The inputs to the HDWI are vapor pressure deficit (a function of temperature and humidity) and wind speed. The minimum possible value for

HDWI is 0. Fires are more likely to spread rapidly and have devastating effects when the HDWI is relatively high (Srock et al., 2018). This relative value is important, as no set value indicates high fire risk since different sites will have different relative values of HDWI. Data resolution, regional climate, and other factors affect what is considered to be a high value (McDonald et al., 2018).

Here, we assess the behavior of the HDWI over time with two datasets. Over the past 22 years (2002–2023), the meteorological tower at the National Renewable Energy Laboratory's (NREL's) National Wind Technology Center collected measurements of winds, temperature, and moisture at NREL's Flatirons Campus in Boulder County, Colorado (Aitken et al., 2014). Although these data are well-calibrated and directly represent the conditions at the NREL site on the Boulder County Front Range, they have a limited temporal scope and also cannot represent how fire behavior varies in other locations around the state. To address these spatial and temporal variability issues, we also consider 66 years of ERA5 reanalysis data spanning the state of Colorado. Reanalysis data represent an integration of numerous data sources (but not including the NREL tower) with weather forecasts to provide an assessment of weather over a wide spatial and temporal range (Jeppesen, 2023).

Additionally, we address discrepancies in wind speed measurements between the observational data and reanalysis data. We analyze a third dataset, the WIND Toolkit from NREL, to analyze the role of spatial resolution in recorded wind speed values. The WIND Toolkit data are available between 2007 and 2012 but do not include any moisture measurements, making calculation of the HDWI impossible for this dataset. The refined temporal and spatial resolution in the WIND Toolkit allows us to explore the role of spatial resolution in wind speed estimation.

This paper is organized as follows: Section 2 summarizes the datasets. In Section 3, we explain how the HDWI is calculated from the datasets, including a discussion of temporal averaging. Results from the NREL tower and from the ERA5 reanalysis, including significance testing, can be found in Section 4. Discussion and conclusions are found in Section 5.

Chapter 2

Datasets

2.1 Observational Data

NREL hosts several meteorological towers in Boulder County as part of its field wind turbine testing efforts. The M2 tower has the longest continuous data record (Clifton and Lundquist, 2012). Since 2002, measurements have been collected every 2 seconds and averaged over 1 minute. Between 1996 and 2002, data are averaged every 10 minutes. The tower is located at 39° 54' 38.34" N, 105° 14' 5.28" W (Figures 2.1 and 2.2). Measurements include temperature at 2 m, 50 m, and 80 m; dew point at 2 m; and wind speeds at 2 m, 5 m, 10 m, 20 m, 50 m, and 80 m. Temperatures are measured with Met One model T-200A platinum resistance thermometers. The dew point is measured using a Michell model SF52 dew point transmitter inside a fan-aspirated radiation shield. Wind speed is measured by cup anemometers (Met One model WS-201 Wind System) at the six elevations. The data used in this study ranged from 1 January 2002 to 31 December 2023 (Jager and Andreas, 1996). We note that while this twenty-two year duration dataset is not as long as the 30-year period used by the World Meteorological Organization to quantify climate, several other studies have analyzed climate trends over shorter periods for fire weather (Levin and Saaroni, 1999; Crimmins, 2006) and wind energy (Millstein et al., 2022) applications.

The calculation of the HDWI requires daily maximum vapor pressure (VPD) deficit and wind speed measurements taken in the lowest 500 m above ground level (Srock et al., 2018). To calculate VPD, both temperature and dew point are needed, so the 2-m measurements are used. We use the maximum wind speed of all the wind elevations available (usually the 80-m measurement) for our

HDWI calculations.

Wind speed measurements, on average, generally increase as measurement height increases (Landberg, 2015) except when patterns such as low-level jets occur (Banta et al., 2002; Vanderwende et al., 2015). Because our analysis is constrained to winds from 80-m elevation, and calculation of HDWI from other sites could consider winds up to a 500-m elevation, the absolute values and distribution of the HDWI from the M2 tower should only be compared to other HDWI values at M2, not to other sites.

Figure 2.1: Aerial view of the National Renewable Energy Laboratory's Flatirons Campus showing the M2 meteorological tower on the west edge of the campus. (Photo by Josh Bauer/Bryan Bechtold, NREL)

2.1.1 Observational Data Quality Control

We apply data quality control to the NREL M2 data. As downloaded from the site, missing values are assigned numeric values of -999999 or 999999. In other cases, recorded measurements are erroneous. We further filter the data in two stages. The first stage involves setting realistic upper and lower limits on values. Temperature readings are constrained to between -52° C and 46° C, the record low and high, respectively, for Colorado (Anderson, 2022). Wind speeds are constrained to between 0 and 90 m/s, as 201 mph is the fastest recorded wind gust in Colorado

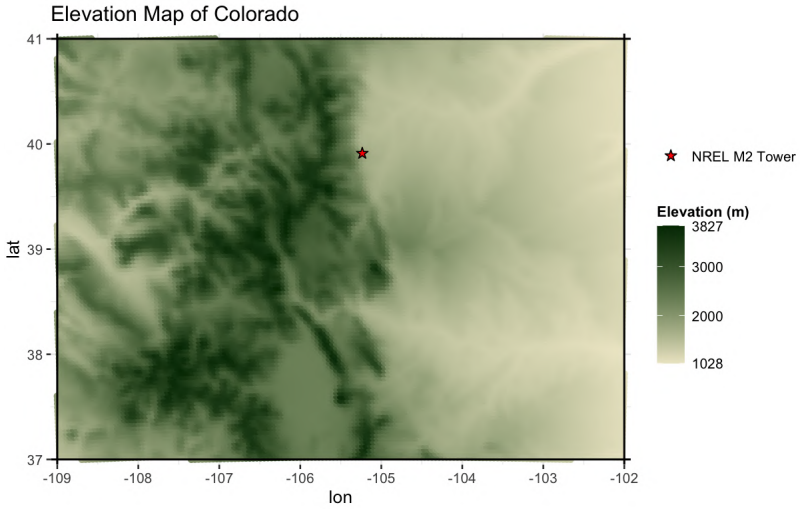

Figure 2.2: Elevation map of Colorado marked with the location of the NREL M2 tower.

(McKee, 2021). Any temperatures and wind speeds not within that range are noted in a separate column and not used in the data analysis. About 0.076% of the data were removed during this stage (around 400 points out of more than 500,000 total points per year). The second stage of filtering involves marking any values within 5 indices (5 minutes) on either end of a noted erroneous value in another column, assuming data points near errors may also be subject to instrument error. An additional 0.038% of the data were removed during this step. After these two filtering steps, more than 99.8% of the original data remain.

2.1.2 Vapor Pressure Deficit

VPD is calculated from temperature and dew point measurements at 2 m using

$$VPD = e_s - e \tag{2.1}$$

where e_s is the saturation vapor pressure and e is the actual vapor pressure (Seager et al., 2015).

Vapor pressures e_s and e can be approximated from temperature and dew point measurements, measured at the NREL tower. The value of e_s can be approximated by

$$e_s = e_0 \exp[\frac{L}{R_v}(\frac{1}{T_0} - \frac{1}{T_K})] \tag{2.2}$$

where T_K is the temperature in Kelvin (Stull, 2017). Appendix A provides the values of the constants.

Vapor pressure e can be approximated using Equation (2.2) but by using the dew point temperature instead of the temperature T_K.

2.1.3 Sustained Wind Speed

To adjust HDWI calculations for observational data, rather than the model forecast data for which it was designed, we reconsider the definition of maximum wind speed. When using forecast data, or in this case 6-hourly reanalysis data, the maximum wind speed for the day is considered to be the fastest wind speed out of four 6-hour periods: midnight to 6 a.m., 6 a.m. to noon, noon to 6 p.m., and 6 p.m. to midnight (Worsnop et al., 2020). Coarse data like reanalysis data cannot predict short wind gusts due to temporal smoothing, but data observed every minute will include such gusts. This difference in measurement will affect the calculation of the HDWI, often producing a large HDWI because a short but unsustained wind gust may affect the observed data.

To distinguish sustained winds from gusts, the National Weather Service defines **sustained wind speed** as the minimum wind speed over 2 minutes (NOAA, 2009). We follow this definition and choose the minimum sustained wind over a 2-minute period to minimize temporal smoothing. The maximum wind speed for the day is then the maximum sustained wind speed across all time points for that day.

2.2 Reanalysis Data

In the absence of observational data over the entire state or for a longer time period, we use ERA5 reanalysis data to extend the spatial and temporal scope of this data analysis (Hersbach et al., 2020). Reanalysis data assimilates observational data and prior weather forecasts into forecasting models to provide a best-case characterization of atmospheric state (Jeppesen, 2023). Because of the lack of long-term observational sites throughout the states, the use of renalaysis data is required.

ERA5 data are available starting 1 January 1940 in 1-hour increments. We analyze ERA5

reanalysis data starting on 1 January 1957 due to inconsistencies in wind measurements in the data before 1957 (Mu et al., 2024). The data are available at every 0.25 degree of longitude and latitude. We consider data within Colorado's state lines: 37° N to 41° N and 102° W to 109° W, or 493 unique ERA5 data points.

At each of these points, the daily HDWI is calculated as the product of maximum vapor pressure deficit and maximum wind speed. These quantities are calculated from 100-m u (west-to-east) component of wind, 100-m v (south-to-north) component of wind, 10-m u component of wind, 10-m v component of wind, 2-m dew point temperature, and 2-m temperature.

As with observational data, VPD is calculated from the temperature and the dew point from the reanalysis data (Equations 2.1 and 2.2). The maximum wind speed is the higher wind speed at a given time point between the 10-m and 100-m measurements, with the maximum usually happening at the 100-m altitude.

2.3 WIND Toolkit Data

WIND Toolkit data from NREL are available at many sites. Like reanalysis data, WIND Toolkit data is simulated. Hourly wind speed measurements at 2km × 2km resolution are available from 2007 – 2012 across the continental United States. We collect all data points within the bounds of 39.875° N – 40.125° N and -105.375° W – -105.125° W. Relative humidity or any other measure of moisture is not available in this dataset, so HDWI cannot be calculated. We use the Wind Toolkit wind data to compare to reanalysis winds.

Chapter 3

Methodology

3.1 Wind Speed Distributions

Reanalysis data is often negatively biased compared to observations (Hallgren et al., 2020; Wilczak et al., 2024). This slow bias would affect the calculations of the HDWI since wind speed is an input for HDWI. To assess this bias, we first fit Weibull distributions using maximum likelihood estimation to the daily maximum wind speeds for both the observational data and the reanalysis data for the years 2007 – 2012. Weibull distributions have been shown to fit wind speed distributions relatively strongly (Justus et al., 1976). Because the temporal resolution for the observational data is much finer than that of the reanalysis data, observed wind speeds are also averaged over 1-hour intervals and fitted with a new Weibull distribution.

To address the impact of the coarse spatial resolution of the reanalysis data, we compare the reanalysis wind speed distributions to that of a more spatially refined modeled dataset, the WIND Toolkit dataset. We first calculate the daily maximum wind speed from the WIND Toolkit at 40 ° N, 105.25 ° W and fit the values to a Weibull distribution. We then calculate the average hourly wind speed between the 39.875° N – 40.125° N and -105.375° W – -105.125° W, to compare to one reanalysis grid cell, and take the daily maximum from that spatial average. We fit the spatially averaged data to another Weibull distribution and compare the parameters to those from reanalysis point 40 ° N, 105.25 ° W. After fitting distributions to each set of winds, we construct confidence intervals to estimate the bias in average maximum wind speeds between data sets.

3.2 Calculation of the Hot-Dry-Windy Index

The formula for the daily HDWI, defined by Srock et al. (2018), for either observational or reanalysis data is

$$HDWI_S = \max_{24-hr}\{U \times VPD\} \tag{3.1}$$

where U is the maximum wind speed out of all possible elevations within the lowest 500m of the atmosphere in m s^{-1} and VPD is the vapor pressure deficit in hPa at a given time (Srock et al., 2018). The daily HDWI value is the maximum HDWI value out of all HDWI values for a given day. We use the subscript S to stand for "standard", as this was how HDWI was originally defined.

Worsnop et al. (2020) calculated HDWI slightly differently:

$$HDWI_W = \max_{24-hr} U \times \max_{24-hr} VPD \tag{3.2}$$

where $\max_{24-hr} U$ is the daily maximum wind speed (out of all possible elevations and all possible times) in m s^{-1} and $\max_{24-hr} VPD$ is the daily maximum vapor pressure deficit in hPa. The subscript W is used for this alternative formula since it serves as a worst-case-scenario calculation of HDWI. The daily maximum wind speed and the daily maximum water vapor pressure deficit do not need to occur simultaneously in $HDWI_W$.

Using Equations (3.1) and (3.2), we first calculate the daily HDWI values for every day between 1 January 2002 and 31 December 2022 in the observational dataset. The observational dataset has wind speeds up to 80m in altitude, and vapor pressure deficit is only available at the surface (2m). Then, we decompose the time series into three components: trend, seasonality, and random noise (Kendall and Ord, 1990); this decomposition can be done in almost any programming language. The trend in a time series is the overall direction of the data. The seasonality of a time series is a set pattern of fluctuation that happens over specific periods of time, in this case by season. The random noise is all the fluctuations that cannot be explained by a seasonal cycle that likely occurred due to random chance. The original time series is a sum of the three components. We then test the trend component of this decomposition for significant change as the trend measures

the direction of the data (discussed in the following section).

To enable comparison between observations and reanalysis, we repeat this analysis for the single reanalysis point (40° N, 105.25° W), the closest point to the coordinates of the NREL M2 tower. Since HDWI is a relative measure, the values are standardized for each dataset for better comparison. We analyze two time series with the reanalysis data: the 22-year period (2002–2023) corresponding to the observational data, as well as the extended 67-year period (1957–2023). As with observations, reanalysis data are not available for the entire lowest 500 meters of the atmosphere. Wind speeds are available at 10m and 100m, while VPD is only available at 2m.

To asses how season affects HDWI trends, we bin annual ERA5 data monthly to quantify monthly 5th percentile, median, and 95th percentile HDWI values. Percentiles for each month are compared over time to the same month every year. Percentiles across months are not compared to each other. Monthly maximum and minimum values are not analyzed as they are not robust to outliers. This monthly binning allows us to analyze extreme trends as well as reduce noise and autocorrelation.

Finally, to broaden the reanalysis results across the state of Colorado, we consider the monthly 95th HDWI percentile over time (since 1957) for every ERA5 reanalysis point in Colorado. The 95th percentile focuses on the most extreme fire weather occurrences (Jain et al., 2022).

3.3 HDWI Significance Testing

We test for significance in trends using a modified Mann-Kendall test (Hamed and Rao, 1998). This test is designed to detect any monotonic trend (not necessarily linear) in a time series. A non-parametric test is necessary to avoid assuming a specific shape to the trend, as a non-parametric test does not assume a specific shape to the trend. Other modeling methods, such as ordinary least squares, are less ideal since they assume a shape to the trend, and we could not make any assumptions about the distribution or shape of the data. The Mann-Kendall test is designed to detect an increasing or decreasing trend, even if that trend is not linear.

The original Mann-Kendall test requires there not be any autocorrelation between data points

because it is based on the assumption that every data point is independent of one another. Due to the concern of autocorrelation in time series data, we use the adjusted test, as specified by Hamed and Rao (1998). If there is no autocorrelation in the data, then the results from the adjusted test are the same as those from the original test. If there is autocorrelation, then the modified test yields a more reliable result. There is a possibility of the modified Mann-Kendall test failing due to the trend in the data being non-monotonic, but this failure did not occur in any of our significance tests. We assign the tests a significance level, $\alpha = 0.05$.

The hypotheses are defined as follows:

$$H_0 : \text{there is not a trend in the data; } H_1 : \text{there is a trend in the data}$$

The more tests we perform, the more likely we are to get false positives. Since multiple tests will be performed, we employ the Benjamini-Hochberg procedure to control the number of false positives (Benjamini and Hochberg, 1995). While each test is not necessarily independent, the procedure still works since they are not negatively dependent.

Chapter 4

Results

4.1 Wind Speeds

Wind speeds in reanalysis data, such as ERA5, often exhibit a slow bias compared to observations (Wilczak et al., 2024). We first establish that our selection of ERA5 data is negatively biased compared to observations. We then investigate whether this bias is caused by temporal or spatial resolution. To do this, we compare the Weibull distributions of daily maximum wind speeds.

We first investigate how the distribution of maximum reanalysis wind speeds differ from the distribution of maximum observed wind speeds. We fit each distribution of maximum wind speeds to a Weibull distribution with shape parameter k and scale parameter θ using maximum likelihood esitmation. Wind speeds typically follow a Weibull distribution with $k \in (1, 3)$ and $\theta \in (1.1\overline{U}, 1.3\overline{U})$ where $\overline{U}$ is the mean wind speed of the data (Justus et al., 1976). (See Appendix B for quantile-quantile plots of the Weibull fits)

We find that the Weibull distribution of daily observed maximum wind speeds has parameters $k = 2.402$ and $\theta = 14.934$ m s^{-1}. On the other hand, the Weibull distribution of daily reanalysis maximum wind speeds has parameters $k = 2.790$ and a much smaller scale parameter of $\theta = 6.149$ m s^{-1} (Figure 4.1). The lower value of θ for the reanalysis data suggests that wind speeds found in reanalysis data are systematically slower than those actually observed. A 95% confidence interval for the average bias between the data sets (1-hr reanalysis − 2-min observations) is (-7.972 m s^{-1}, -7.453 m s^{-1}). This bias is statistically significant since 0 us not a value in the interval.

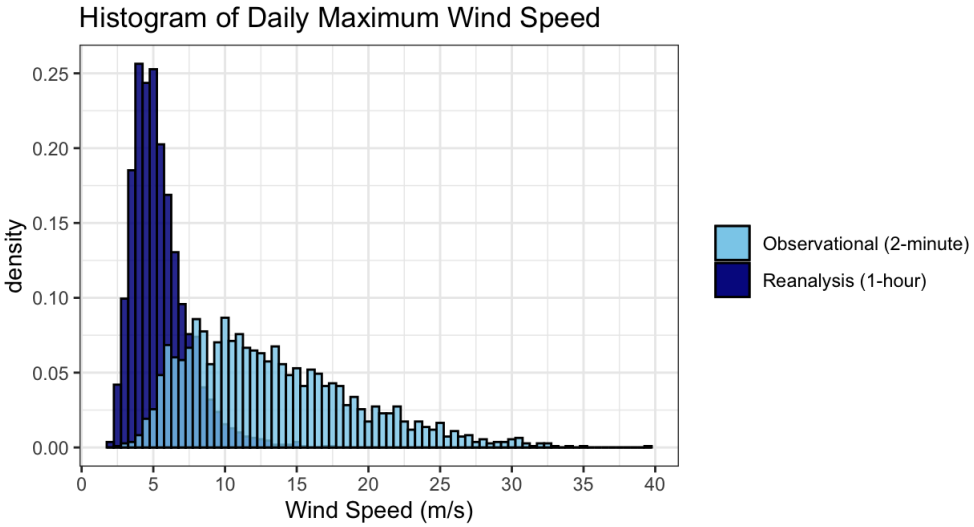

Figure 4.1: Histogram of Daily Maximum Wind Speeds for Observational and Reanalysis Data (2007 – 2012)

One possible explanation for this significant bias is temporal resolution. The observational data has a temporal resolution of 2 minutes, while the reanalysis data has a temporal resolution of 1 hour. Data with coarser temporal resolution may be subject to temporal smoothing and averaging, contributing to a negative bias.

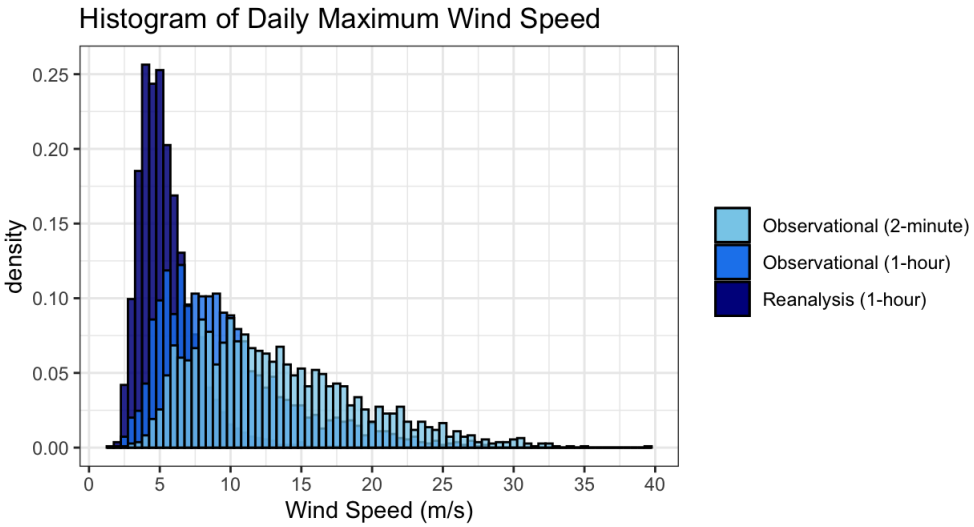

Figure 4.2: Histogram of Daily Maximum Wind Speeds for 2-minute Observational, 1-hour averaged Observational, and Reanalysis Data (2007 – 2012)

We smooth the observational data to 1-hour periods to match the reanalysis data's tempo-

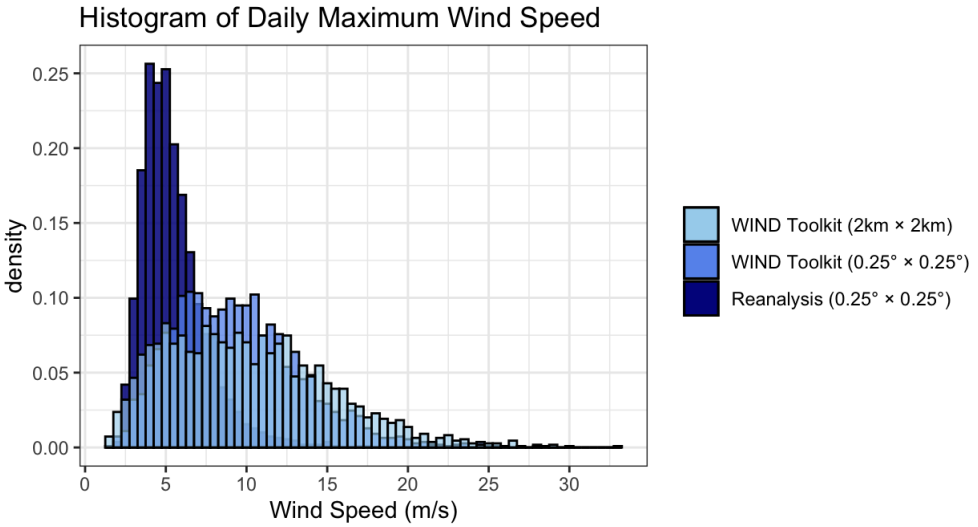

Figure 4.3: Histogram of Daily Maximum Wind Speeds for 2km × 2km WIND Toolkit data, spatially averaged 0.25° × 0.25° WIND Toolkit data, and 0.25° × 0.25° Reanalysis data (2007 – 2012)

ral resolution and refit with a Weibull distribution to investigate if temporal resolution explains the negative bias in reanalysis wind speeds. We do this by averaging the wind speed over the hour. Temporally smoothed observational maximum wind speeds have a Weibull distribution with parameters $k = 2.219$ and $\theta = 10.984$ m s^{-1} (Figure 4.2). A 95% confidence interval for the average bias between the reanalysis and observational data, each with 1-hour resolution, is $(-4.416$ m s^{-1}, -3.992 m s$^{-1})$. While this bias for temporally smoothed observational wind speeds is less compared to the 2-min resolution observations, temporal resolution does not fully explain the systematic bias.

A second possible explanation for the reanalysis slow bias is spatial resolution. Similar to temporal smoothing and averaging, data can also be smoothed and averaged spatially. To investigate the role of spatial resolution in recorded wind speeds, we compare the reanalysis data point at 40° N, 105.25° W to a point in the exact same location from the WIND Toolkit data. The spatial resolution of reanalysis data is 0.25° × 0.25°, which is about 111km × 85km, while the spatial resolution of the WIND Toolkit data is much finer at 2km × 2km. Both the reanalysis data and the WIND Toolkit data have 1-hour temporal resolutions.

The Weibull distribution of maximum wind speeds according to WIND Toolkit data has shape parameters $k = 2.118$ and scale parameter $\theta = 11.409$ m s^{-1}. The bias between the reanalysis data and the WIND Toolkit data is again significant, with a 95% confidence interval for the average bias being (-4.821 m s^{-1}, -4.366 m s^{-1}). When the WIND Toolkit data is spatially smoothed over a $0.25° \times 0.25°$ grid cell, the parameters are $k = 2.511$ and $\theta = 10.628$ m s^{-1} (Figure 4.3). These spatially smoothed WIND Toolkit data and the reanalysis data have the same spatial and temporal resolution, and yet, they yield significantly different values of scale parameter θ. A 95% confidence interval for the average bias is (-4.120 m s^{-1}, -3.747 m s^{-1}). Therefore, the underestimation bias present in the reanalysis data is not completely explained by either differences in spatial or in temporal resolution. We note that other investigators have also found a slow bias in ERA5 winds (Pronk et al., 2022; Wilczak et al., 2024). Recognizing this slow bias in the winds that consistute the HDWI, we now assess trends in the HDWI.

4.2 Daily HDWI Trends

4.2.1 Observational Data

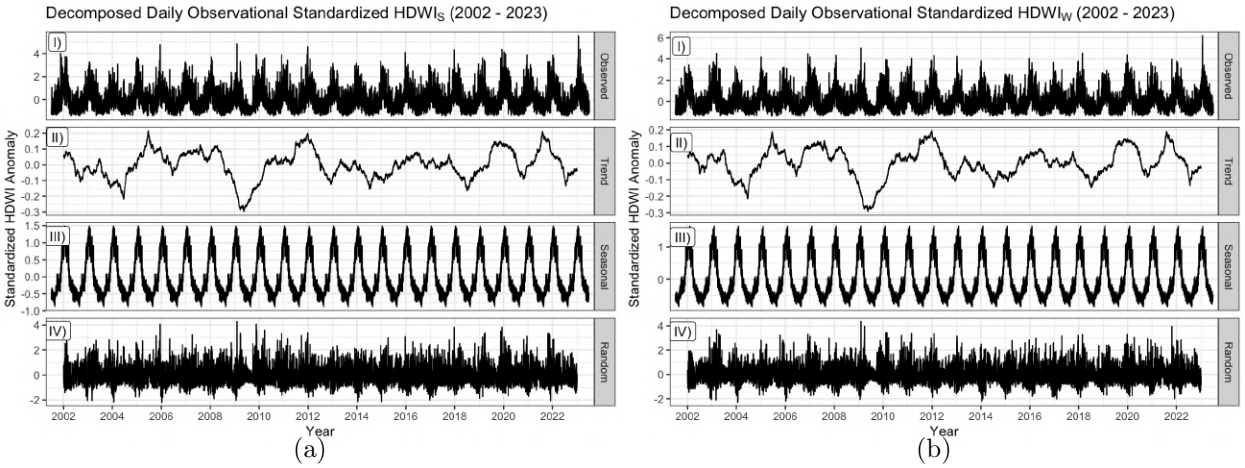

Figure 4.4: Time series decomposition of standardized $HDWI_S$ (a) and $HDWI_W$ (b) values for observational data (2002–2023). (I) Observed raw data; (II) trend that was extracted and analyzed; (III) seasonality; (IV) random noise. The sum of panels (II)–(IV) add up to panel (I).

First, we standardize the HDWI values. We then decompose the time series of HDWI values

calculated from observational data into its components of trend, seasonality, and random noise for both the $HDWI_S$ and $HDWI_W$ calculations (Figure 4.4) and perform the modified Mann-Kendall test on the trend component of the data to analyze if there is a statistically significant change in fire weather occurrences.

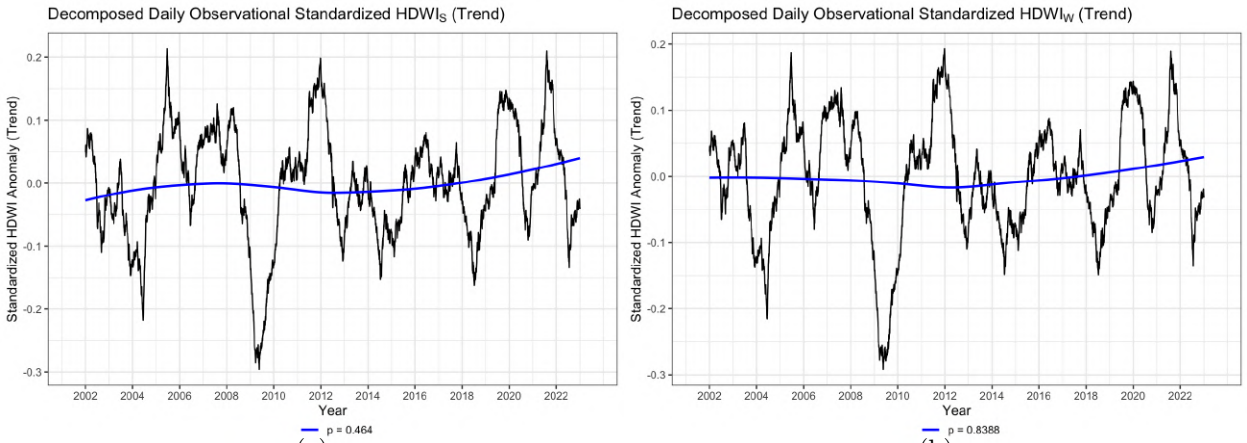

(a) (b)

Figure 4.5: Standardized trend component from time series decomposition of observational $HDWI_S$ (a) and $HDWI_W$ (b) values (2002–2023). Fitted with loess estimator (moving weighted average). The trends are not statistically significant with $p > \alpha = 0.05$

The observational data fail to demonstrate a significant trend in fire weather occurrences on the daily level, regardless of the method used to calculate $HDWI$ (Figure 4.5). While there appears to be a slight increase starting around 2012 for both $HDWI_S$ and $HDWI_W$, neither are statistically significant—the respective Mann-Kendall tests have $p = 0.464$ and $p = 0.8388$. This result may be surprising, as rising global temperatures are well-documented (Jain et al., 2022). Twenty-two years is perhaps insufficiently long to detect a trend, necessitating the need for another data source to extend the time series. ERA5 reanalysis data are fairly consistent since 1957 (Mu et al., 2024).

4.2.2 Reanalysis Data

We first analyzed the corresponding 22-year (2002–2023) reanalysis trend component. We use the reanalysis point with coordinates 40° N, 105.25° W, the point closest to the NREL tower. Unlike

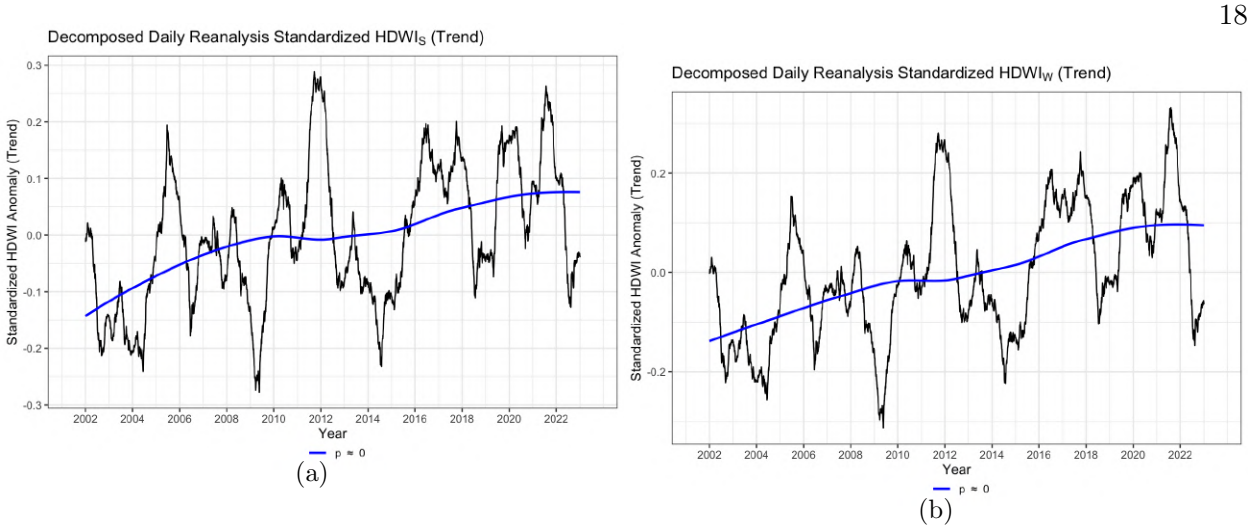

Figure 4.6: Standardized trend component from time series decomposition of reanalysis $HDWI_S$ (a) and $HDWI_W$ (b) values (2002–2023). Fitted with loess estimator (moving weighted average). The trends are statistically significant with $p < \alpha = 0.05$

the observational data, the ERA5 data indicate a significant increase in $HDWI_S$ and $HDWI_W$ between 2002 and 2023 with $p \approx 0$ (Figure 4.6). (See Appendix B for time series decomposition graphs for ERA5 data.) This difference in statistical significance is likely due to differences between wind measurements (Appendix D).

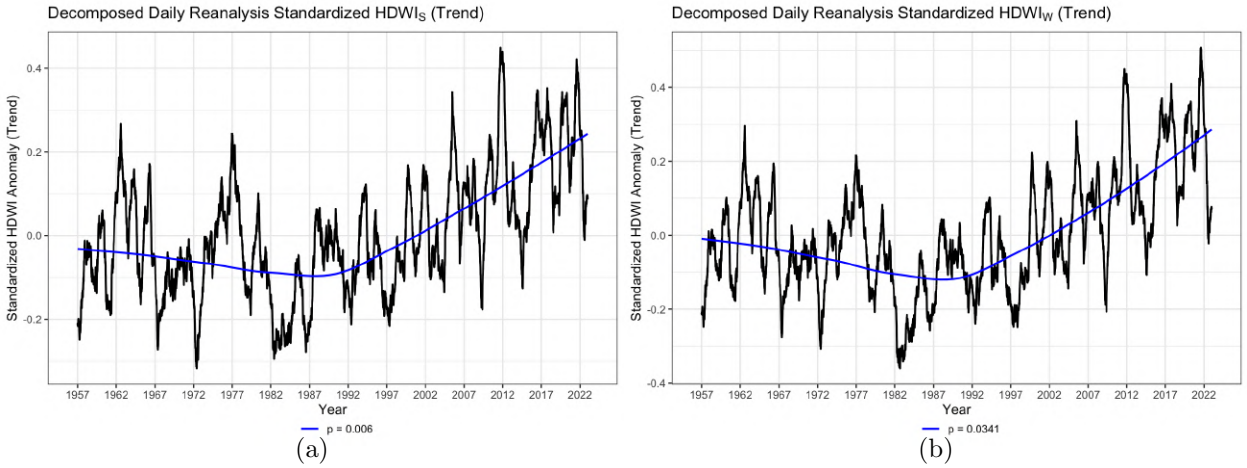

Figure 4.7: Standardized trend component from time series decomposition of reanalysis $HDWI_S$ (a) and $HDWI_W$ (b) values (1957–2023). Fitted with loess estimator (moving weighted average). The trends are statistically significant with $p < \alpha = 0.05$

One advantage of using the ERA5 dataset in addition to the observational dataset is the

possibility of considering a longer time period. Extending the reanalysis data to the 66-year time series (1957–2022) also shows a significant increase in $HDWI_S$ and $HDWI_W$ at $\alpha = 0.05$. (Figure 4.7). A sharply increasing trend appears to begin around 1990.

4.3 Monthly HDWI Trends

Another benefit of having a longer time series is the ability to analyze monthly patterns to investigate whether fire weather occurrences are increasing more in specific months. Sixty-seven years of ERA5 reanalysis data (1957 – 2023) at coordinates 40° N, 105.25° W are binned monthly and analyzed for increasing occurrences of fire weather. Since many significance tests are conducted, statistical significance is adjusted according to the Benjamini-Hochberg procedure to lower false positives (Benjamini and Hochberg, 1995). This lowers the significance level of each individual test in order to keep the entire set of tests at significance $\alpha = 0.05$. Individual tests significant at $\alpha = 0.05$ but not after applying the Benjamini-Hochberg procedure are still noted.

Table 4.1: Table of p-values for $HDWI_S$ (ERA5 reanalysis data, 1957–2023). Boldface indicates a significant increase; italics, a significant decrease. ** indicates significance according to the Benjamini-Hochberg procedure; * indicates significance at $\alpha = 0.05$ only. Plain text indicates no statistically significant trends.

	5th Percentile	50th Percentile	95th Percentile
January	0.074	0.849	0.114
February	0.247	0.974	0.689
March	**0.019** *	**0.005** **	**0.041** *
April	0.238	0.138	0.313
May	0.35	0.474	**0.01** **
June	**0.003** **	**0** **	0.057
July	**0.013** **	**0** **	**0** **
August	**0.002** **	**0** **	**0** **
September	**0.001** **	**0.045** *	**0.034** *
October	0.721	**0.013** **	0.132
November	0.341	**0.043** *	0.974
December	0.367	0.311	**0.027** *

Table 4.2: Table of p-values for $HDWI_W$ (ERA5 reanalysis data, 1957–2023). Boldface indicates a significant increase; italics, a significant decrease. ** indicates significance according to the Benjamini-Hochberg procedure; * indicates significance at $\alpha = 0.05$ only. Plain text indicates no statistically significant trends.

	5th Percentile	50th Percentile	95th Percentile
January	0.058	0.991	0.423
February	0.269	1	0.649
March	**0.004** **	**0** **	**0.046** *
April	0.194	0.642	0.449
May	0.405	0.633	**0.027** **
June	0.058	**0.001** **	0.053
July	**0.044** *	**0.001** **	**0** **
August	**0.013** **	**0.001** **	**0.007** **
September	**0.018** *	**0.012** **	**0.008** **
October	0.991	0.261	0.304
November	0.314	0.1918	0.802
December	0.145	0.565	**0.032 ***

Strong evidence of increasing $HDWI_S$ and $HDWI_W$ emerges across many months and percentiles (Tables 4.1 and 4.2). Notably, every percentile in August was statistically significant, for both $HDWI_S$ and $HDWI_W$. An increase in the 5th percentile suggests that the lowest values are increasing, meaning that the number of days with low fire risk is decreasing. An increase in the 95th percentile suggests indicates that extreme trends are becoming even more extreme, meaning that on some days, fires will spread even more than they would have used to. Figure 4.8 shows trends in August, all of which are statistically significant. (see Appendix E for figures for other months). Seeing all percentiles of HDWI increase for the month of August over the 67-year time period (1957 – 2023) provides some evidence of fire season worsening, as August has previously been a month of peak fire weather occurrences (Balch et al., 2018). While there is some evidence of increasing fire weather occurrences in September, but the results are inconclusive according to this dataset.

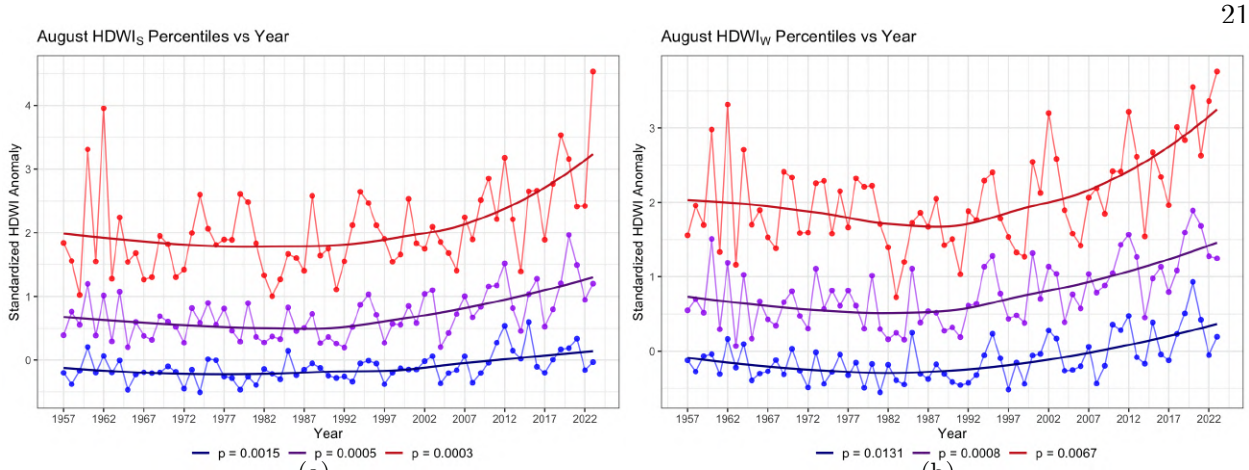

(a) (b)

Figure 4.8: Time series of standardized August $HDWI_S$ (a) and $HDWI_W$ (b) percentiles (5th, 50th, 95th) from 1957 to 2023. Fitted with loess estimators. The trends are statistically significant

4.4 HDWI Trends Across All of Colorado

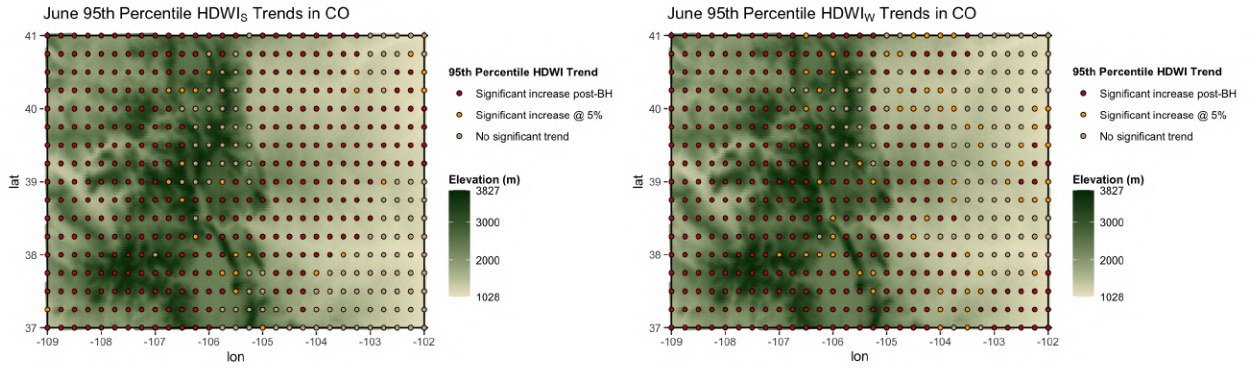

(a) (b)

Figure 4.9: June 95th percentile $HDWI_S$ (a) and $HDWI_W$ (b) test results for trends across all of Colorado.

Another advantage to considering reanalysis data is its wide spatial scope, enabling assessment of changing fire weather occurrences across the entire state of Colorado, whose population is rapidly growing. We focus on the 95th percentile to capture the most extreme fire weather conditions (Jain et al., 2022).

There is some evidence of widespread increases in extreme fire weather occurrences between 1957 and 2023—both under standard calculations and worst-case calculations, especially in summer months, such as June (Figure 4.9). (See Appendix F for figures for remaining 11 months). Increasing trends in other months tend to be spatially dependent. In the winter months (December, January, February), there is not conclusive evidence of worsening extreme conditions.

Chapter 5

Discussion and Conclusions

Recognizing the impact of fire weather occurrences on Colorado's growing population, this study investigates changing HDWI patterns in Colorado using 22 years of observational data and up to 67 years of reanalysis data. The observational data comes from NREL's meteorological tower M2 on Colorado's Front Range; the reanalysis dataset is the ERA5 dataset. While reanalysis data is widely available, it may not be as useful for fire managers like the U. S. Forest Service because of its distinct difference from observational data, primarily in terms of its slow wind speed bias. Because wind speeds from reanalysis data have a slow bias compared to observations, we analyze the differences in distributions of daily maximum wind speeds for each and investigate the role of spatial and temporal resolution in this bias. We find that temporal resolution partially explains the negative bias while spatial resolution plays very little into that bias. However, even when matching spatial and temporal resolution, the average maximum wind speed for reanalysis data remains significantly slower compared to other datasets. Other recent studies assessing reanalysis winds (not using this site) also find a slow bias (Pronk et al., 2022; Wilczak et al., 2024).

To analyze fire weather occurrences, we decompose the datasets into trend, seasonality, and random noise components, and assess the trends for statistical significance. Modified Mann-Kendall significance tests on the observational data (2002 – 2023) do not indicate an increasing trend in fire weather occurrences. On the other hand, reanalysis data on the same 22-year timescale does show a statistically significant increasing trend. This contrast between the two datasets can mainly be attributed to the differences in wind speed measurements (Appendix C).

The lack of a trend from observational data appears to contradict results from prior research. However, these prior results assess global trends using reanalysis data rather than examining localized measurements, considering the rarity of extended observational datasets. Jain et al. (2022) considered global fire trends, as opposed to local trends, and they considered a 41-year time series of reanalysis data. Additionally, Westerling et al. (2006) found that a majority of the increases in fire weather occurrences occur during the 1980s, a time period which is not part of the data collected at NREL. Weatherhead et al. (1998) noted that the smaller the true change in a trend, the more years of data are required take to detect the change with statistical certainty. Changes like rising temperatures are small and gradual, but a small increase in temperature can have a large environmental impact. More years of data are needed for a conclusive result.

In contrast, using the same approach, an extended 66-year ERA5 time series does indicate increasing trends in fire weather occurrences due to significantly increasing $HDWI_S$ and $HDWI_W$ values. According to the reanalysis data, a statistically significant increasing trend in fire weather occurrences is present at the daily level. When the reanalysis data are binned monthly, significant increases in HDWI occur for at least one percentile for 10 of the 12 months of the year when analyzing all 66 years. Importantly for the summertime fire season, HDWI significantly increases at all percentiles during later summer months (July, August, September). By extending the time series to 67 years using the reanalysis data, our results became more consistent with results from previous research suggesting increasing fire weather occurrences.

Although the average global temperature has increased over time, which in turn would increase the vapor pressure deficit and overall fire risk, this trend does not seem to be the case locally in the Colorado Front Range when analyzing observational data, at least at this specific site. Public perceptions of increasing fire weather occurrences may be due more to the impact of fires rather than actual increases in the frequency of fire weather occurrences. Also, the $HDWI$ only considers weather effects on fire weather occurrences, without considering the state of possible fire fuels. Other fire weather indices which consider the state of fuels, may present a different assessment of whether or not fire likelihood is increasing.

A future study could involve a more detailed comparison between reanalysis data and observational data, ideally comparing observational and reanalysis data at multiple sites. Further, although the $HDWI$ may be applied to any type of data, some questions about its use remain. In particular, the dependence of significance test results on the approach for dealing with high-frequency (gusty) wind measurements from observations. Here, we required a 2-minute sustained gust from our observations. The sensitivity to this time period could be assessed.

Finally, while we address fire initiation weather here, an extension could assess how the frequency and magnitude of actual fires in Colorado are changing over time. While the fire risk has been seemingly steady between 2002 and 2023, that does not mean that actual fire frequency and damage have also stayed steady. Fire ignition events, from lightning or anthropogenic sources, have their own trends that affect fire occurrences. The characteristics of vegetation and other fuels for fires could also be considered.

Bibliography

Aitken, M. L., R. M. Banta, Y. L. Pichugina, and J. K. Lundquist, 2014: Quantifying Wind Turbine Wake Characteristics from Scanning Remote Sensor Data. *Journal of Atmospheric and Oceanic Technology*, **31 (4)**, 765–787, https://doi.org/10.1175/JTECH-D-13-00104.1.

Anderson, Z., 2022: The Most Extreme Temperatures In Colorado's History. *iHeart*.

Balch, J. K., T. Schoennagel, A. P. Williams, J. T. Abatzoglou, M. E. Cattau, N. P. Mietkiewicz, and L. A. St. Denis, 2018: Switching on the Big Burn of 2017. *Fire*, **1 (1)**, 17, https://doi.org/10.3390/fire1010017.

Banta, R. M., R. K. Newsom, J. K. Lundquist, Y. L. Pichugina, R. L. Coulter, and L. Mahrt, 2002: Nocturnal Low-Level Jet Characteristics Over Kansas During Cases-99. *Boundary-Layer Meteorology*, **105 (2)**, 221–252, https://doi.org/10.1023/A:1019992330866.

Benjamini, Y., and Y. Hochberg, 1995: Controlling the False Discovery Rate: A Practical and Powerful Approach to Multiple Testing. *Journal of the Royal Statistical Society*, **57 (1)**.

Blumhardt, M., 2020: Cameron Peak Fire's long and historic run leaves stories of miracles and misery. *Fort Collins Coloradoan*.

Brasch, S., and J. Wertz, 2023: Xcel Energy tells shareholders Marshall fire lawsuits could seriously hurt its finances. *Colorado Public Radio*.

Clifton, A., and J. K. Lundquist, 2012: Data Clustering Reveals Climate Impacts on Local Wind Phenomena. *Journal of Applied Meteorology and Climatology*, **51 (8)**, 1547–1557, https://doi.org/10.1175/JAMC-D-11-0227.1.

Crimmins, M. A., 2006: Synoptic climatology of extreme fire-weather conditions across the southwest United States. *International Journal of Climatology*, **26 (8)**, 1001–1016, https://doi.org/10.1002/joc.1300.

Flynn, C., 2022: Nearly 1,100 homes destroyed in Marshall Fire, valued at over $500 million. *FOX31 Denver*.

Gabbert, B., 2022: US Forest Service says Colorado's East Troublesome Fire was human caused. *Wildfire Today*.

Hallgren, C., J. Arnqvist, S. Ivanell, H. Körnich, V. Vakkari, and E. Sahlée, 2020: Looking for an Offshore Low-Level Jet Champion among Recent Reanalyses: A Tight Race over the Baltic Sea. *Energies*, **13 (14)**, 3670, https://doi.org/10.3390/en13143670.

Hamed, K. H., and A. R. Rao, 1998: A modified Mann-Kendall trend test for autocorrelated data. *Journal of Hydrology*, **204 (1-4)**, 182–196, https://doi.org/10.1016/S0022-1694(97)00125-X.

Hersbach, H., and Coauthors, 2020: The ERA5 global reanalysis. *Quarterly Journal of the Royal Meteorological Society*, **146 (730)**, 1999–2049, https://doi.org/10.1002/qj.3803.

Jager, D., and A. Andreas, 1996: NREL National Wind Technology Center (NWTC): M2 Tower; Boulder, Colorado (Data). Tech. Rep. NREL Report No. DA-5500-56489, NREL, Golden, CO. URL `http://dx.doi.org/10.5439/1052222`.

Jain, P., D. Castellanos-Acuna, S. C. P. Coogan, J. T. Abatzoglou, and M. D. Flannigan, 2022: Observed increases in extreme fire weather driven by atmospheric humidity and temperature. *Nature Climate Change*, **12 (1)**, 63–70, https://doi.org/10.1038/s41558-021-01224-1.

Jeppesen, J., 2023: Fact sheet: Reanalysis. *ECMWF*, 2.

Justus, C. G., W. R. Hargraves, and A. Yalcin, 1976: Nationwide Assessment of Potential Output from Wind-Powered Generators.

Kendall, M., and J. K. Ord, 1990: *Time Series*. 3rd ed., Oxford University Press.

Landberg, L., 2015: *Meteorology for Wind Energy*. John Wiley and Sons, Incorporated.

Levin, N., and H. Saaroni, 1999: Fire Weather in Israel — Synoptic Climatological Analysis. *GeoJournal*, **47 (4)**, 523–538, https://doi.org/10.1023/A:1007087217249.

Lipari-DiLeonardo, S., 2023: Downslope windstorms in the front range: A 21-year climatological analysis. M.S. thesis, University of Colorado Boulder, 44 pp., URL `colorado.idm.oclc.org/login?url=https://www-proquest-com.colorado.idm.oclc.org/dissertations-theses/downslope-windstorms-front-range-21-year/docview/2824494944/se-2`.

McDonald, J. M., A. F. Srock, and J. J. Charney, 2018: Development and Application of a Hot-Dry-Windy Index (HDW) Climatology. *Atmosphere*, **9 (7)**, 285, https://doi.org/10.3390/atmos9070285.

McKee, S., 2021: What's the fastest wind speed ever recorded in Colorado? *The Denver Gazette*.

Millstein, D., M. Bolinger, and R. Wiser, 2022: What can surface wind observations tell us about interannual variation in wind energy output? *Wind Energy*, **25 (6)**, https://doi.org/10.1002/we.2717.

Mu, Y., C. Jones, L. M. V. Carvalho, L. Xue, C. Liu, and Q. Ding, 2024: Pacific decadal oscillation and enso forcings of northerly low-level jets on the eastern andes and precipitation extremes in south america. *in review at Nature Climate and Atmospheric Sciences*.

NOAA, 2009: Sustained wind speed. *National Oceanic and Atmospheric Administration's National Weather Service*.

Phillips, N., 2022: Marshall fire losses now expected to exceed $2 billion — making it the 10th costliest wildfire in U.S. history. *The Denver Post*.

Pronk, V., N. Bodini, M. Optis, J. K. Lundquist, P. Moriarty, C. Draxl, A. Purkayastha, and E. Young, 2022: Can reanalysis products outperform mesoscale numerical weather prediction models in modeling the wind resource in simple terrain? *Wind Energy Science*, **7 (2)**, 487–504, https://doi.org/10.5194/wes-7-487-2022.

Seager, R., A. Hooks, A. P. Williams, B. Cook, J. Nakamura, and N. Henderson, 2015: Climatology, Variability, and Trends in the U.S. Vapor Pressure Deficit, an Important Fire-Related Meteorological Quantity. *Journal of Applied Meteorology and Climatology*, **54 (6)**, 1121–1141, https://doi.org/10.1175/JAMC-D-14-0321.1.

Sharples, J. J., 2022: A note on fire weather indices. *International Journal of Wildland Fire*, **31 (7)**, 728–734, https://doi.org/10.1071/WF21134.

Srock, A. F., J. J. Charney, B. E. Potter, and S. L. Goodrick, 2018: The Hot-Dry-Windy Index: A New Fire Weather Index. *Atmosphere*, **9 (7)**, 279, https://doi.org/10.3390/atmos9070279.

Stull, R., 2017: *Practical Meteorology: An Algebra-based Survey of Atmospheric Science*. Univ. of British Columbia, 940 pp., URL `https://www.eoas.ubc.ca/books/Practical_Meteorology/`.

US Census, 2023: U.s. population trends return to pre-pandemic norms as more states gain population. *United States Census Bureau*.

Vanderwende, B. J., J. K. Lundquist, M. E. Rhodes, E. S. Takle, and S. L. Irvin, 2015: Observing and Simulating the Summertime Low-Level Jet in Central Iowa. *Monthly Weather Review*, **143 (6)**, 2319–2336, https://doi.org/10.1175/MWR-D-14-00325.1.

Weatherhead, E. C., and Coauthors, 1998: Factors affecting the detection of trends: Statistical considerations and applications to environmental data. *Journal of Geophysical Research: Atmospheres*, **103 (D14)**, 17 149–17 161, https://doi.org/10.1029/98JD00995.

Westerling, A. L., H. G. Hidalgo, D. R. Cayan, and T. W. Swetnam, 2006: Warming and Earlier Spring Increase Western U.S. Forest Wildfire Activity. *Science*, **313 (5789)**, 940–943, https://doi.org/10.1126/science.1128834.

Wilczak, J. M., E. Akish, A. Capotondi, and G. P. Compo, 2024: Evaluation and Bias Correction of the ERA5 Reanalysis over the United States for Wind and Solar Energy Applications. *Energies*, **17 (7)**, 1667, https://doi.org/10.3390/en17071667.

Worsnop, R. P., M. Scheuerer, F. D. Giuseppe, C. Barnard, T. M. Hamill, and C. Vitolo, 2021: Probabilistic Fire Danger Forecasting: A Framework for Week-Two Forecasts Using Statistical Postprocessing Techniques and the Global ECMWF Fire Forecast System (GEFF). *Weather and Forecasting*, **36 (6)**, 2113–2125, https://doi.org/10.1175/WAF-D-21-0075.1.

Worsnop, R. P., M. Scheuerer, and T. M. Hamill, 2020: Extended-Range Probabilistic Fire-Weather Forecasting Based on Ensemble Model Output Statistics and Ensemble Copula Coupling. *Monthly Weather Review*, **148 (2)**, 499–521, https://doi.org/10.1175/MWR-D-19-0217.1.

Appendix A

Vapor Pressure Deficit Equations and Constants

Vapor pressure deficit is calculated using the formula $VPD = e_s - e$ where

$$e_s = e_0 \exp[\tfrac{L}{R_v}(\tfrac{1}{T_0} - \tfrac{1}{T_K})] \text{ and } e = e_0 \exp[\tfrac{L}{R_v}(\tfrac{1}{T_0} - \tfrac{1}{T_{dK}})]$$

The constants e_0, L, R_v, T_0, T_K, and T_{dK} are defined as follows:

- $e_0 = 0.6113$ kPa

- $L = 2.5 * 10^6$ J kg^{-1}, which is the latent heat of vaporization for liquid water

- $R_v = 461$ J K^{-1} kg^{-1}, which is the water-vapor gas constant

- $\frac{L}{R_v} = 5423$ K (solved algebraically)

- $T_0 = 273.15$ K, or 0°C, the freezing point of water

- T_K is the measured temperature (in Kelvin)

- T_{dK} is the dew point (in Kelvin), which is defined to be the temperature at which, given the current relative humidity and atmospheric pressure, the air would become saturated with water vapor. This value is never greater than the actual temperature.

Appendix B

Weibull Quantile-Quantile Plots

Section 4a discussed the Weibull distributon parameter estimation for wind speeds from the datasets. Quantile-quantile plots show the strength of the theorized distribution against the data.

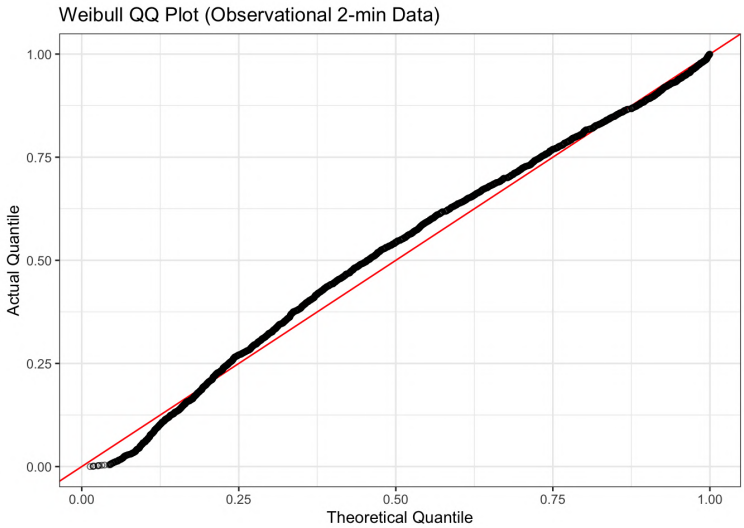

Figure B.1: Quantile-quantile plot showing the fit of a Weibull distribution for maximum daily wind speed from observational data with 2-minute temporal resolution. A perfect fit would be in line with the red line.

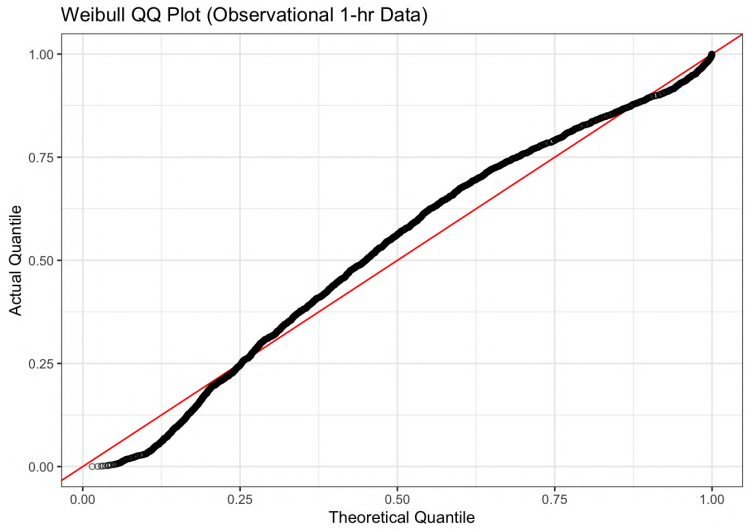

Figure B.2: Quantile-quantile plot showing the fit of a Weibull distribution for maximum daily wind speed from observational data with 1-hour temporal resolution. A perfect fit would be in line with the red line.

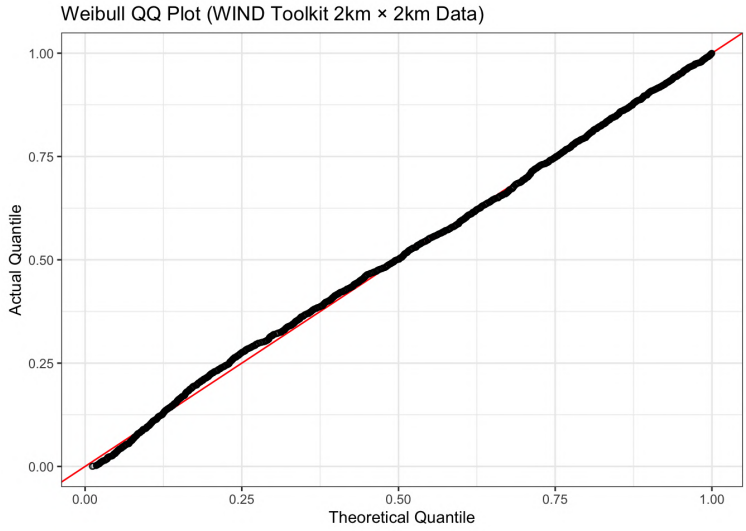

Figure B.3: Quantile-quantile plot showing the fit of a Weibull distribution for maximum daily wind speed from WIND Toolkit data with 2km $\times$ 2km spatial resolution. A perfect fit would be in line with the red line.

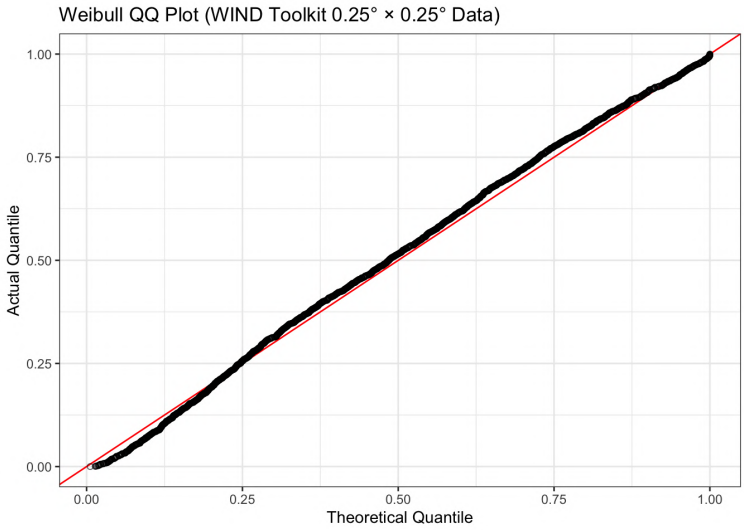

Figure B.4: Quantile-quantile plot showing the fit of a Weibull distribution for maximum daily wind speed from WIND Toolkit data with 0.25° × 0.25 ° spatial resolution. A perfect fit would be in line with the red line.

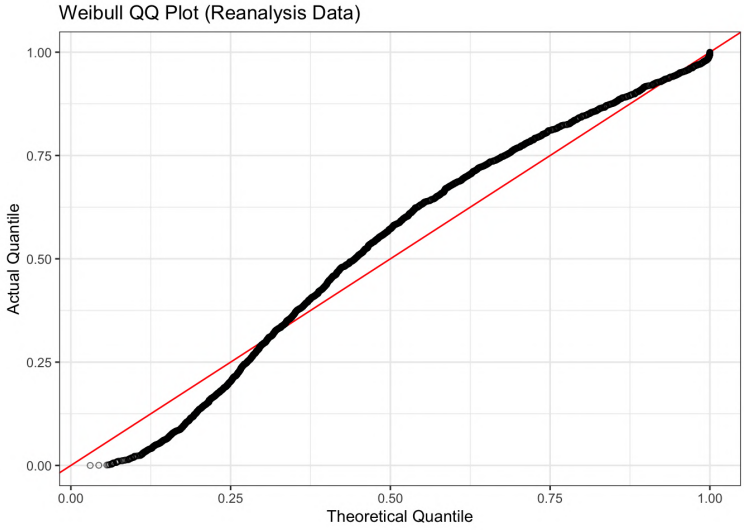

Figure B.5: Quantile-quantile plot showing the fit of a Weibull distribution for maximum daily wind speed from reanalysis data. A perfect fit would be in line with the red line.

Appendix C

Decomposition of daily ERA5 reanalysis data

Figures 4.6 and 4.7 in Section 4 showed the trend component of the time series decomposition of daily ERA5 reanalysis data. The raw data is expressed in panel (I) of Figures C.1 and C.2. Panels (II) - (IV) equal panel (a) when summed. Figures C.1(II) and C.2(II), the trend, was analyzed for significance and displayed in the main body as Figures 4.6 and 4.7.

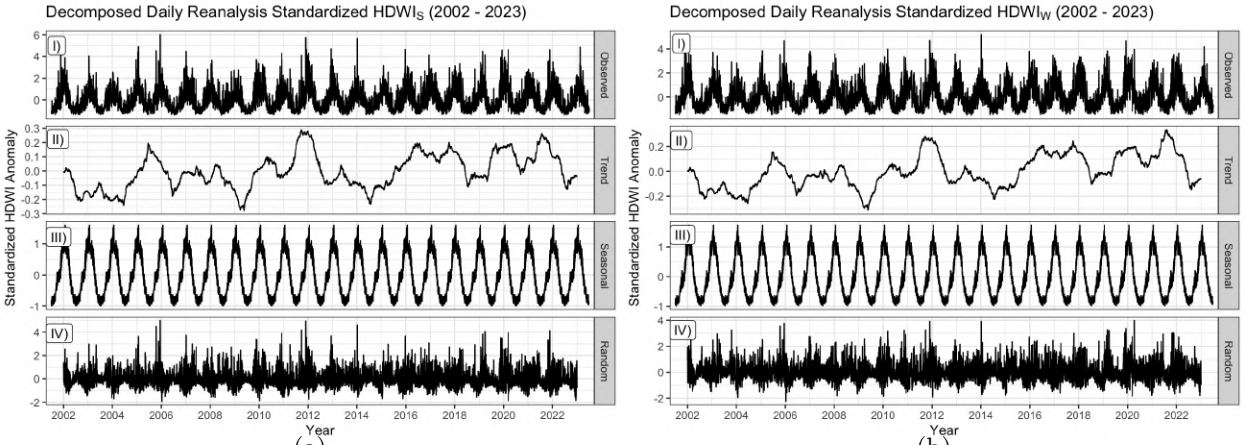

Figure C.1: Time series decomposition of $HDWI_S$ and $HDWI_W$ values for reanalysis data (2002–2023). (I) Observed raw data; (II) trend that was extracted and analyzed; (III) seasonality; (IV) random noise. The sum of panels (II)–(IV) add up to panel (I).

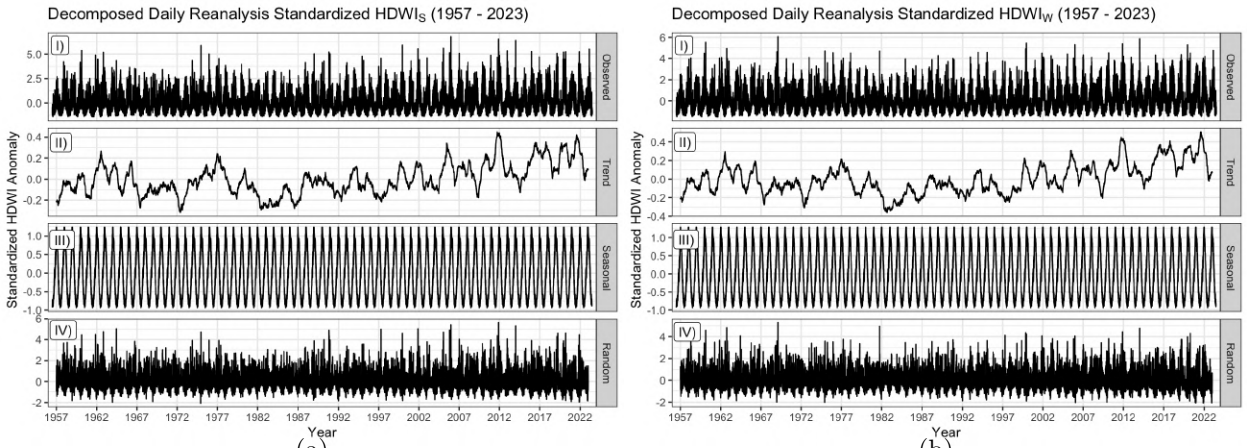

Figure C.2: Time series decomposition of $HDWI_S$ and $HDWI_W$ values for reanalysis data (1957–2023). (I) Observed raw data; (II) trend that was extracted and analyzed; (III) seasonality; (IV) random noise. The sum of panels (II)–(IV) add up to panel (I).

Appendix D

VPD and Wind Analyzed Separately

Section 4(a) discussed how the distribution of wind speeds differed between observational and reanalysis data. Since wind speed is one of the components of HDWI calculations, it would make sense to investigate whether the difference in wind speeds is what caused the difference in statistical significance for HDWI trends in observational and reanalysis data. Lipari-DiLeonardo (2023) analyzed wind data from the NREL M2 weather tower between 2002 and 2021 and found that wind storms in the Colorado Front Range decreased in frequency, duration, and average speed over that 20-year time frame. A decrease in wind storms is highly correlated with a decrease in sustained wind speed. Additionally, Seager et al. (2015) found that VPD increased in the southwest region of the United States during the spring and summer due to increasing values in saturation vapor pressure, also suggesting rising spring and summer temperatures. The HDWI is calculated as a product of wind speed and vapor pressure deficit, so a decrease in one value and an increase in the other value could lead to the relative effects of each cancelling out over time, which may have happened to the observational data.

We first separate the $HDWI_W$ back into maximum VPD and maximum wind speed. We only investigate the differences in $HDWI_W$ components because the two individual daily maxima are independent, wheras the VPD and wind speeds are not independent under the $HDWI_S$ calculation. We decompose the time series of VPD and the wind speed into their additive components of trend, seasonal variation, and random noise. We analyze the trend component using the modified Mann-Kendall test to check if trends are statistically significant.

Observational data from NREL (2002–2023) show a significant decrease in wind speed and a significant increase in VPD. This causes to the $HDWI_W$ to stay relatively consistent over the timespan (Figure D.1). Reanalysis data (2002–2023), on the other hand, indicate a statistically significant increase for both wind speed and VPD (Figure D.2). This provides further evidence that the apparent clash between results is likely due to differences in wind speed measurements between observational and reanalysis data.

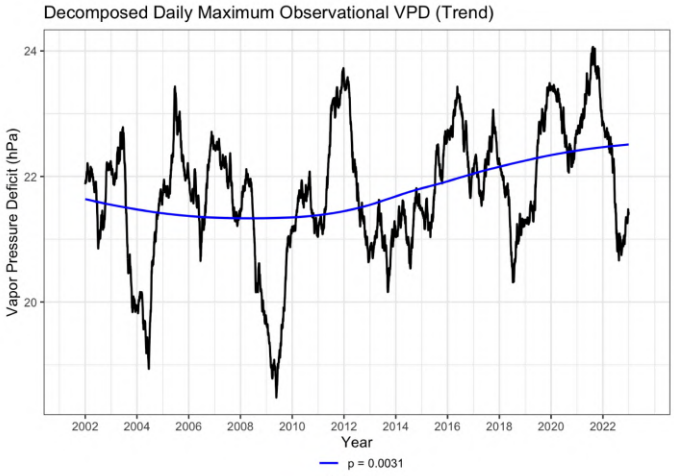

(a)

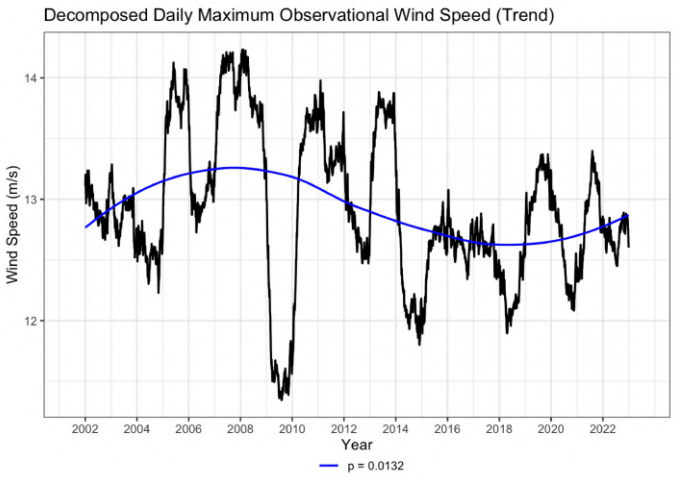

(b)

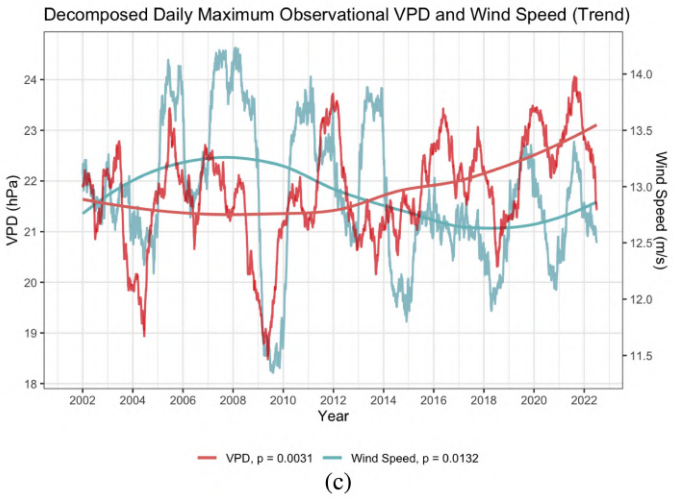

(c)

Figure D.1: Time series (trend) for observational VPD and wind speed from 2002 to 2023: (a) observational VPD; (b) observational wind speed (c) observational VPD and wind speed plotted together

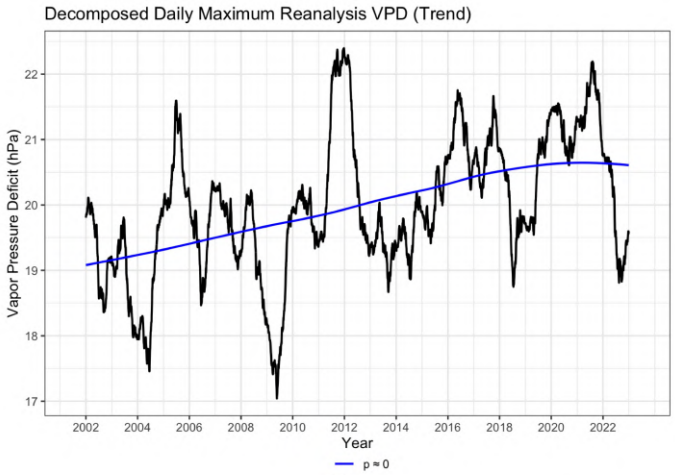

(a)

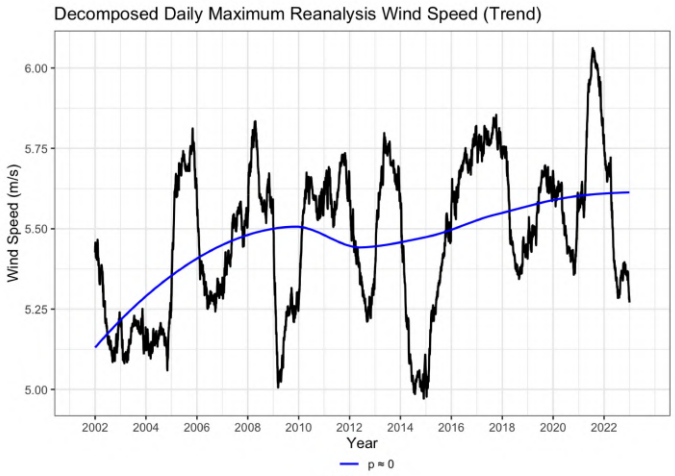

(b)

Figure D.2: Time series (trend) for ERA5 reanalysis VPD and wind speed from 2002 to 2023: (a) reanalysis VPD; (b) reanalysis wind speed

Appendix E

HDWI Percentiles Time Series Figures

The $HDWI_S$ and $HDWI_W$ trends for each month, according to ERA5 reanalysis data from 1957-2023. A solid line indicates significance after Benjamini-Hochberg significance correction, a long dashed line indicates significance at the $\alpha = 0.05$ level, and a short dashed line indicates no significant trend.

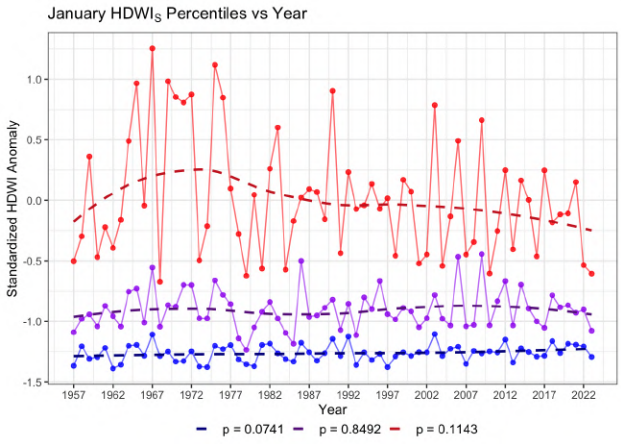

(a) January

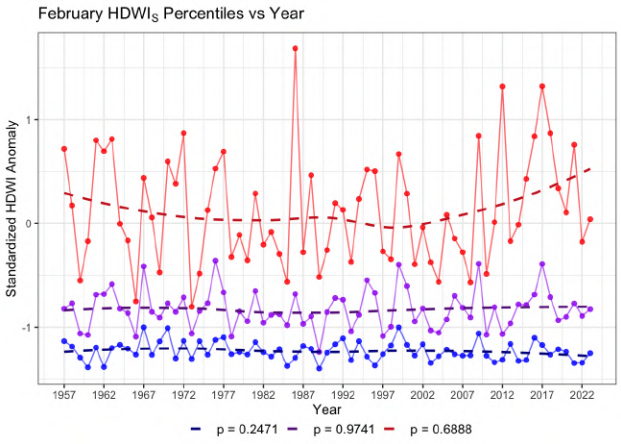

(b) February

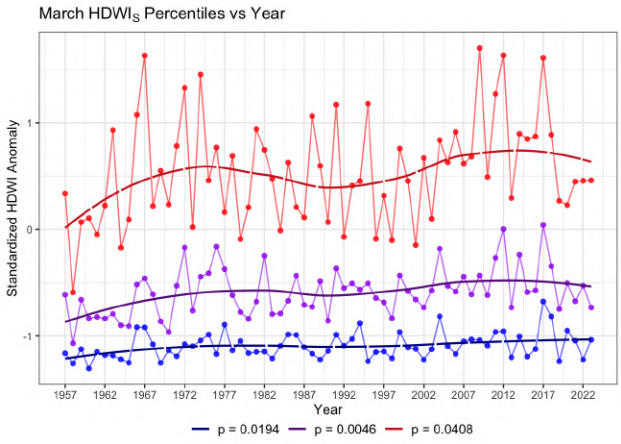

(c) March

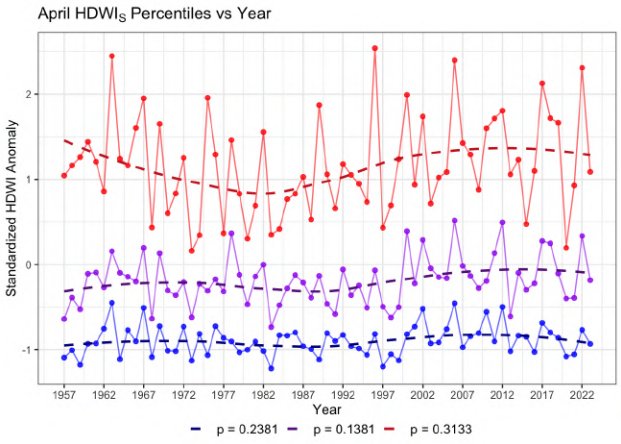

(d) April

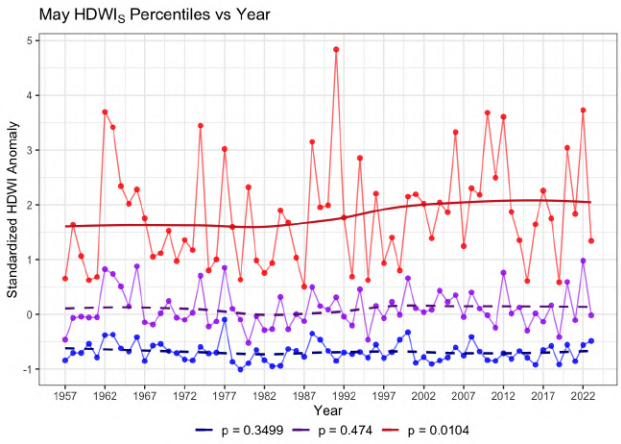

(e) May

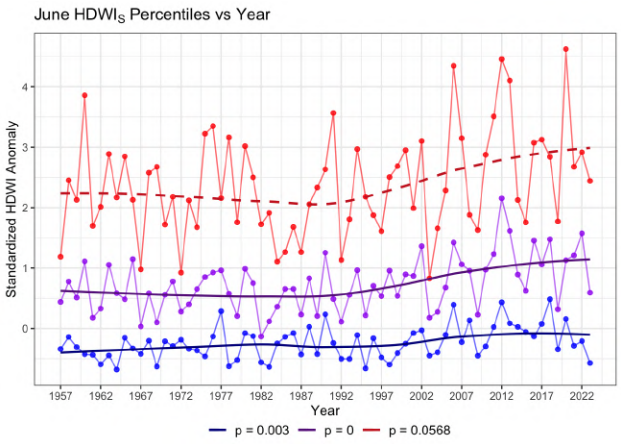

(f) June

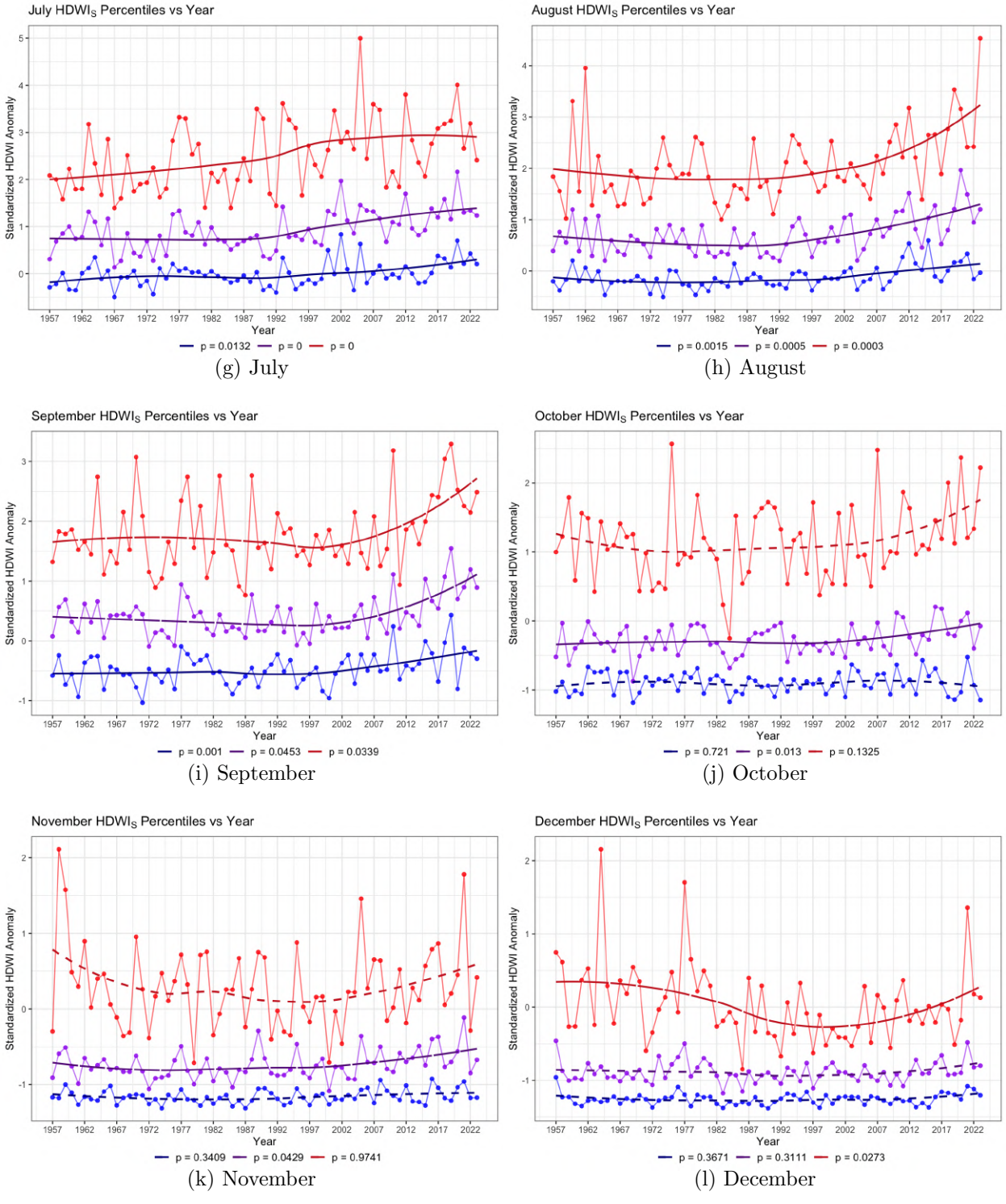

Figure E.1: $HDWI_S$ (1957–2023), all percentiles, ERA5 reanalysis data.

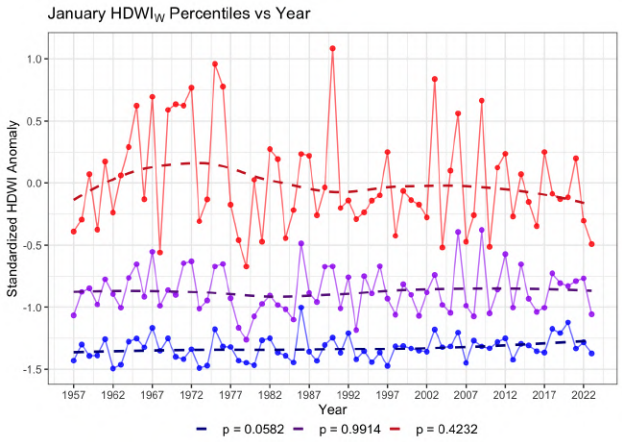

(a) January

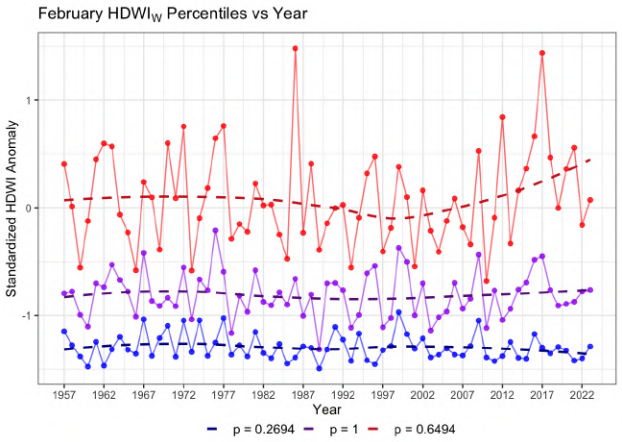

(b) February

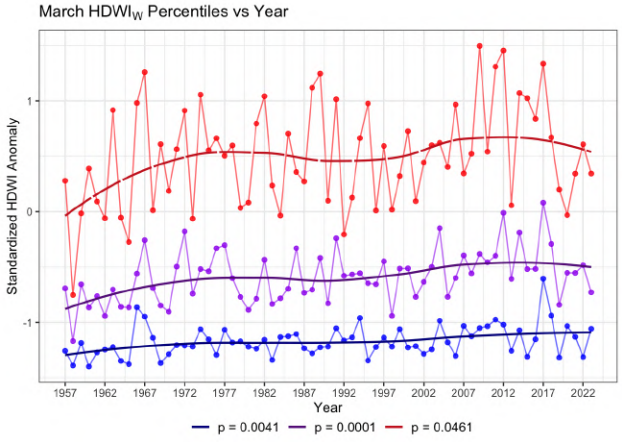

(c) March

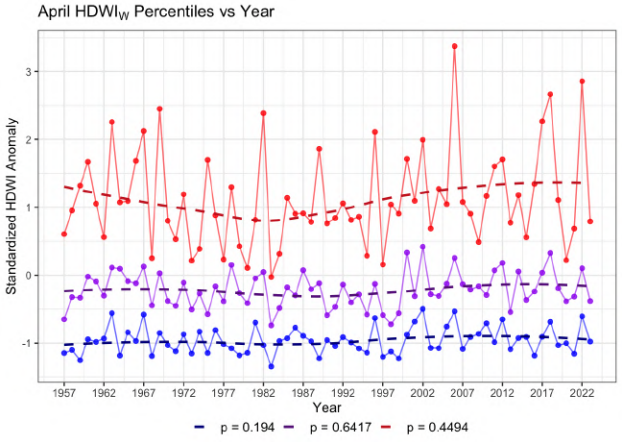

(d) April

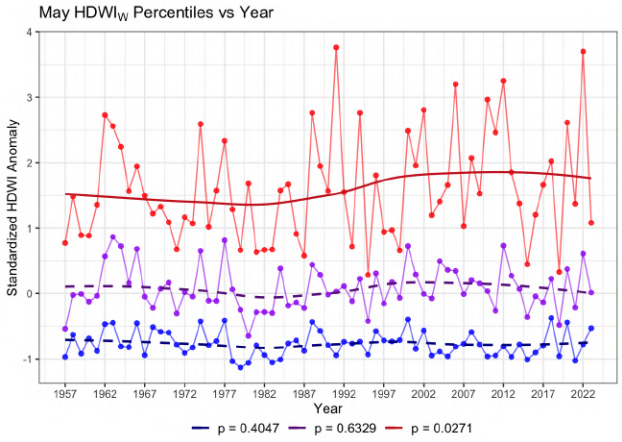

(e) May

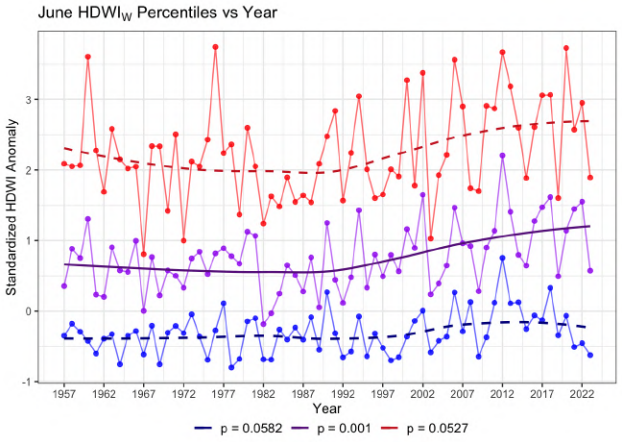

(f) June

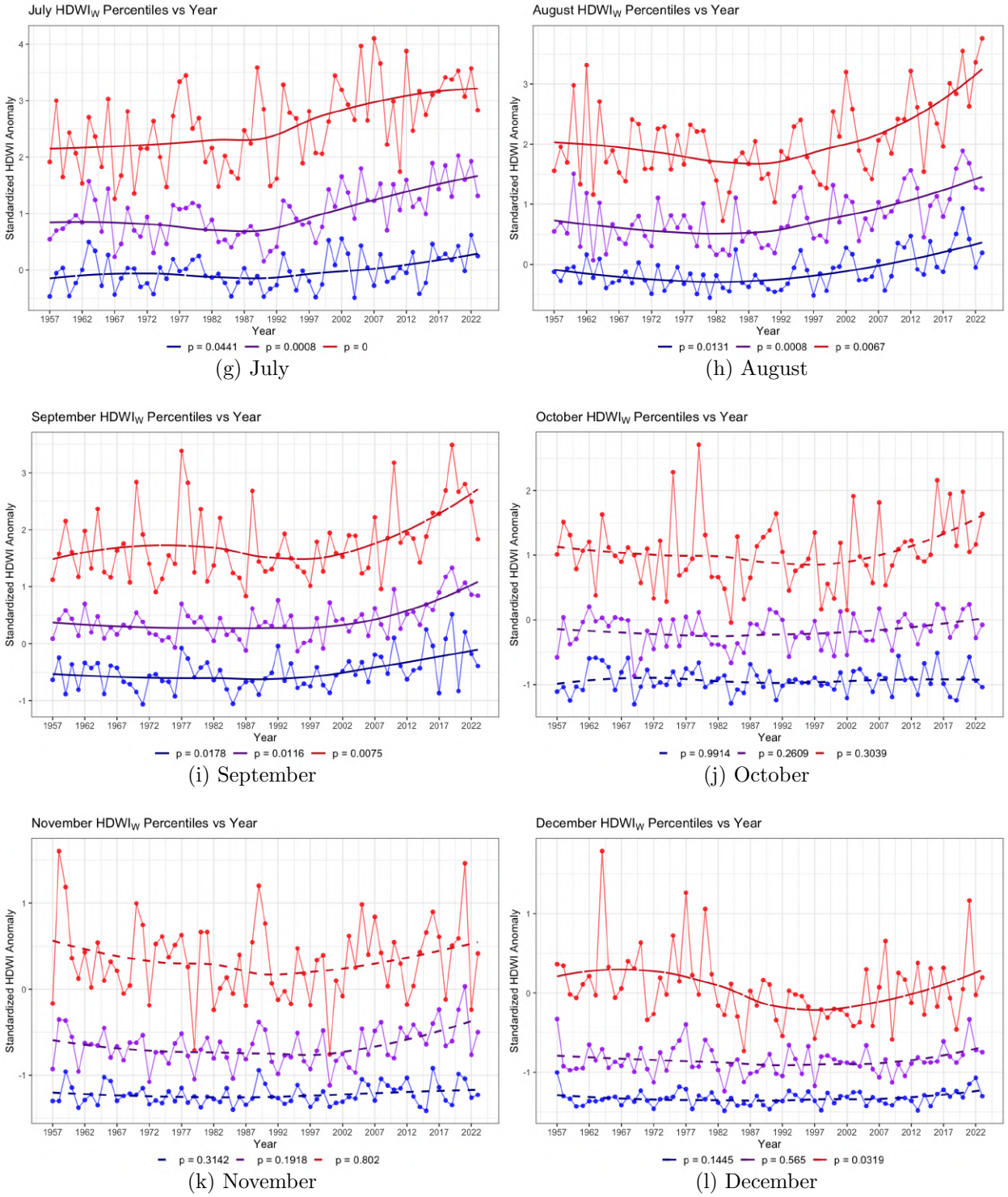

(g) July (h) August

(i) September (j) October

(k) November (l) December

Figure E.2: $HDWI_W$ (1957–2023), all percentiles, ERA5 reanalysis data.

Appendix F

Figures From Colorado

Section 4d discussed analyzing the monthly 95th percentile HDWI value at every reanalysis coordinate in Colorado. Figures F.1 and F.2 show the monthly 95th percentile trends in $HDWI_S$ and $HDWI_W$ between 1957 and 2023. A red dot indicates a significant increase in HDWI after applying the Bejamini-Hochberg correction for statistical significance; orange, a significant increase at $\alpha = 0.05$; tan, no statistical significance; light blue, a significant decrease at $\alpha = 0.05$.

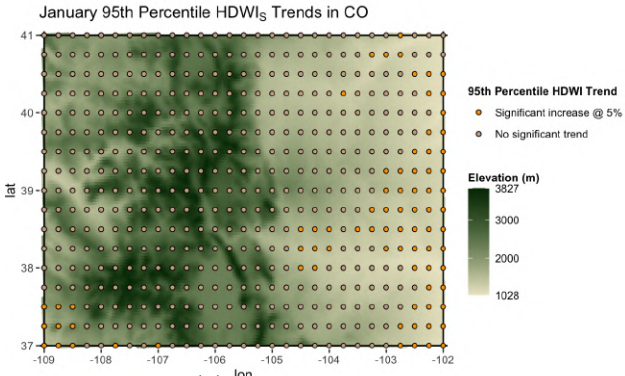

(a) January

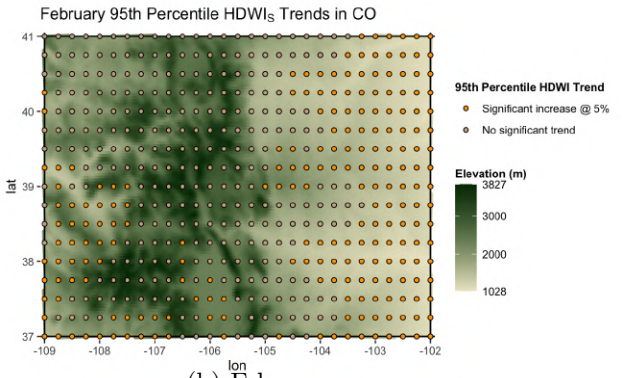

(b) February

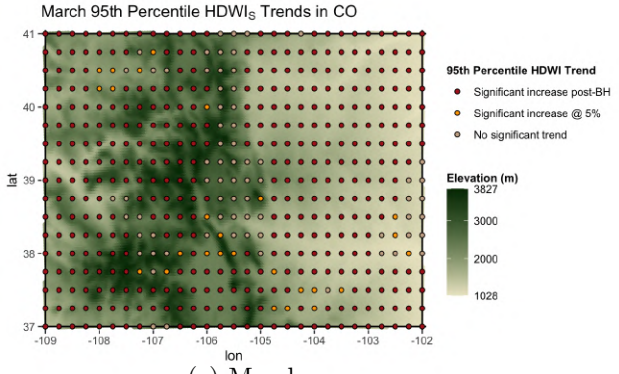

(c) March

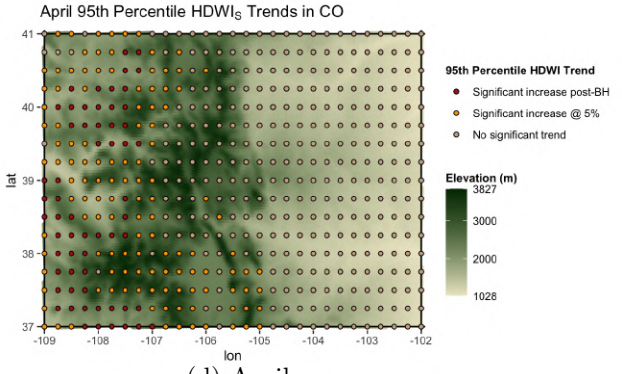

(d) April

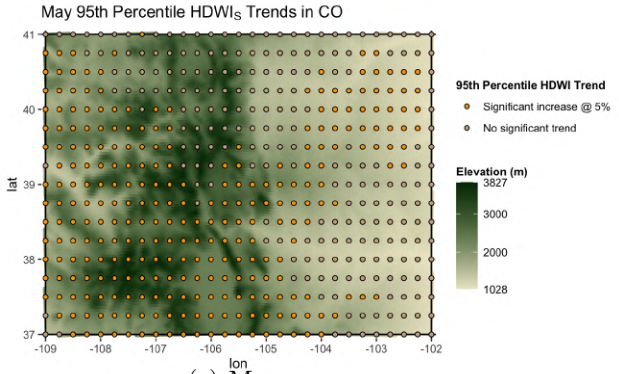

(e) May

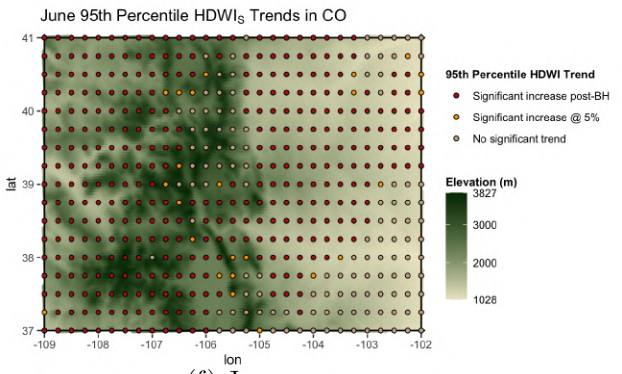

(f) June

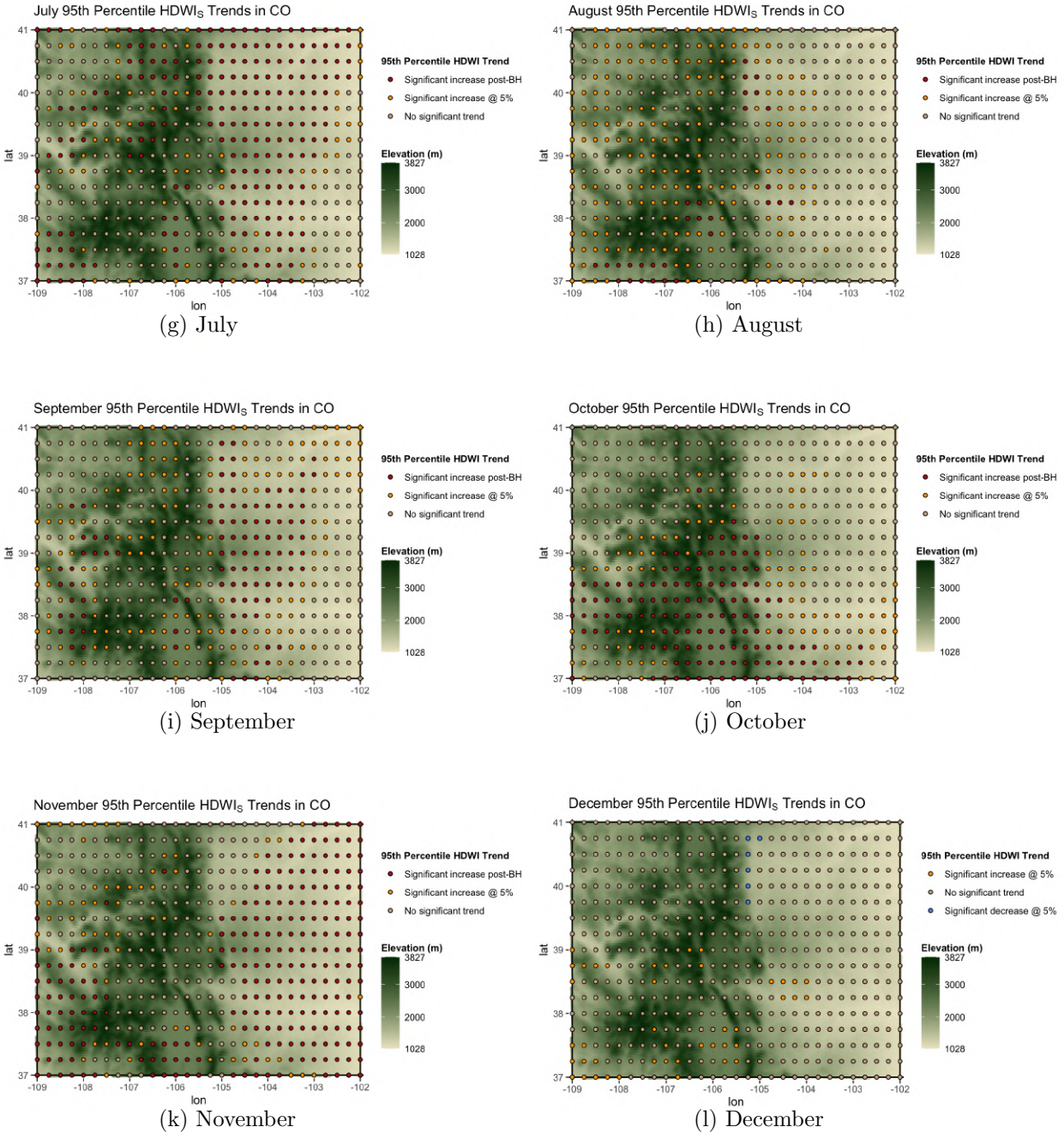

(g) July (h) August

(i) September (j) October

(k) November (l) December

Figure F.1: 95th percentile $HDWI_S$ test results for trends across all of Colorado.

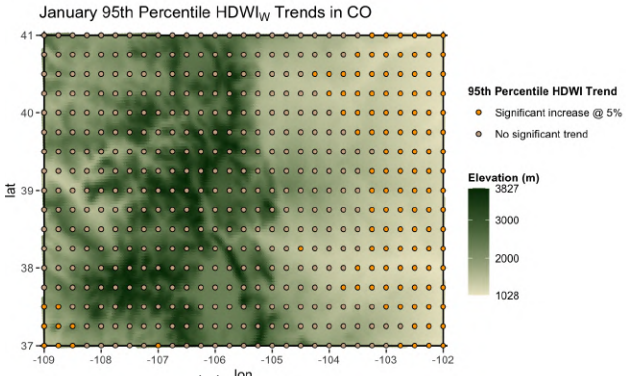

(a) January

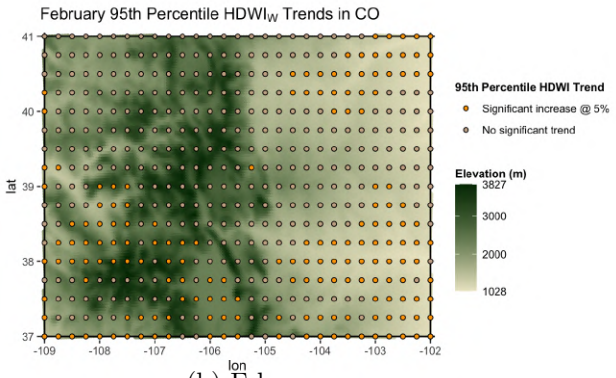

(b) February

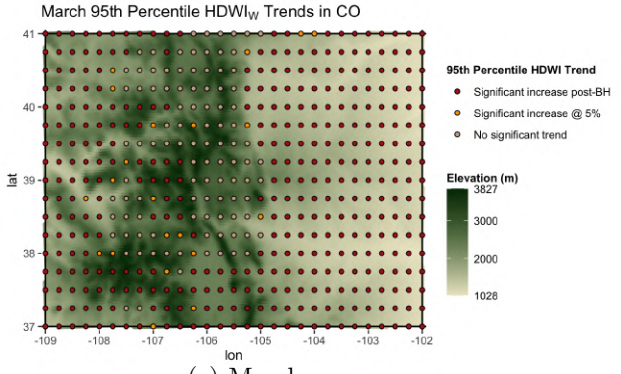

(c) March

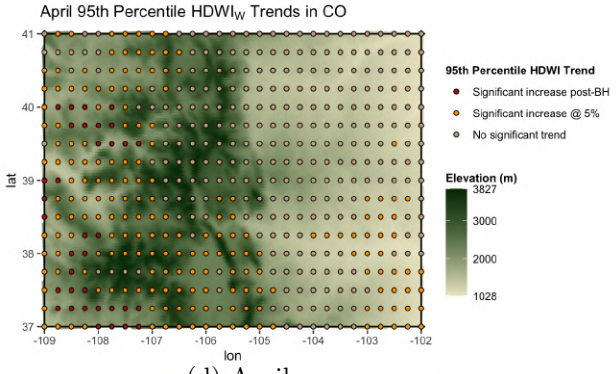

(d) April

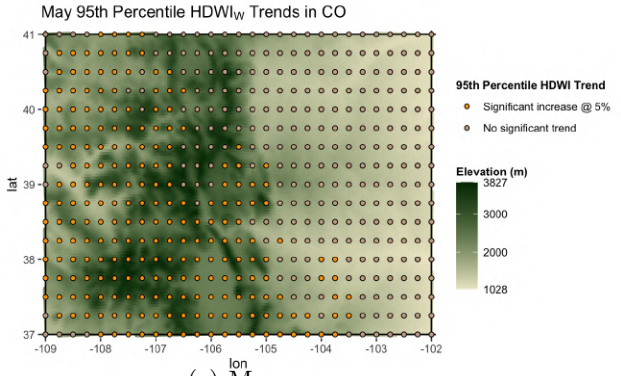

(e) May

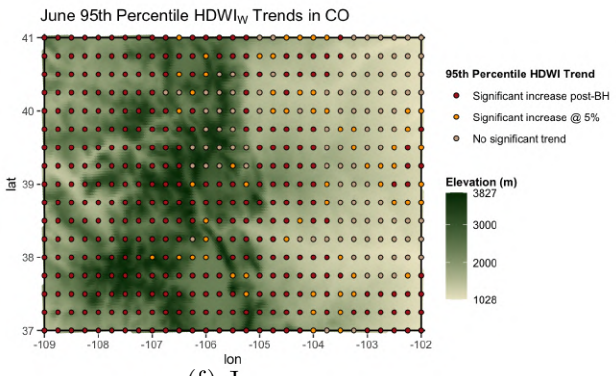

(f) June

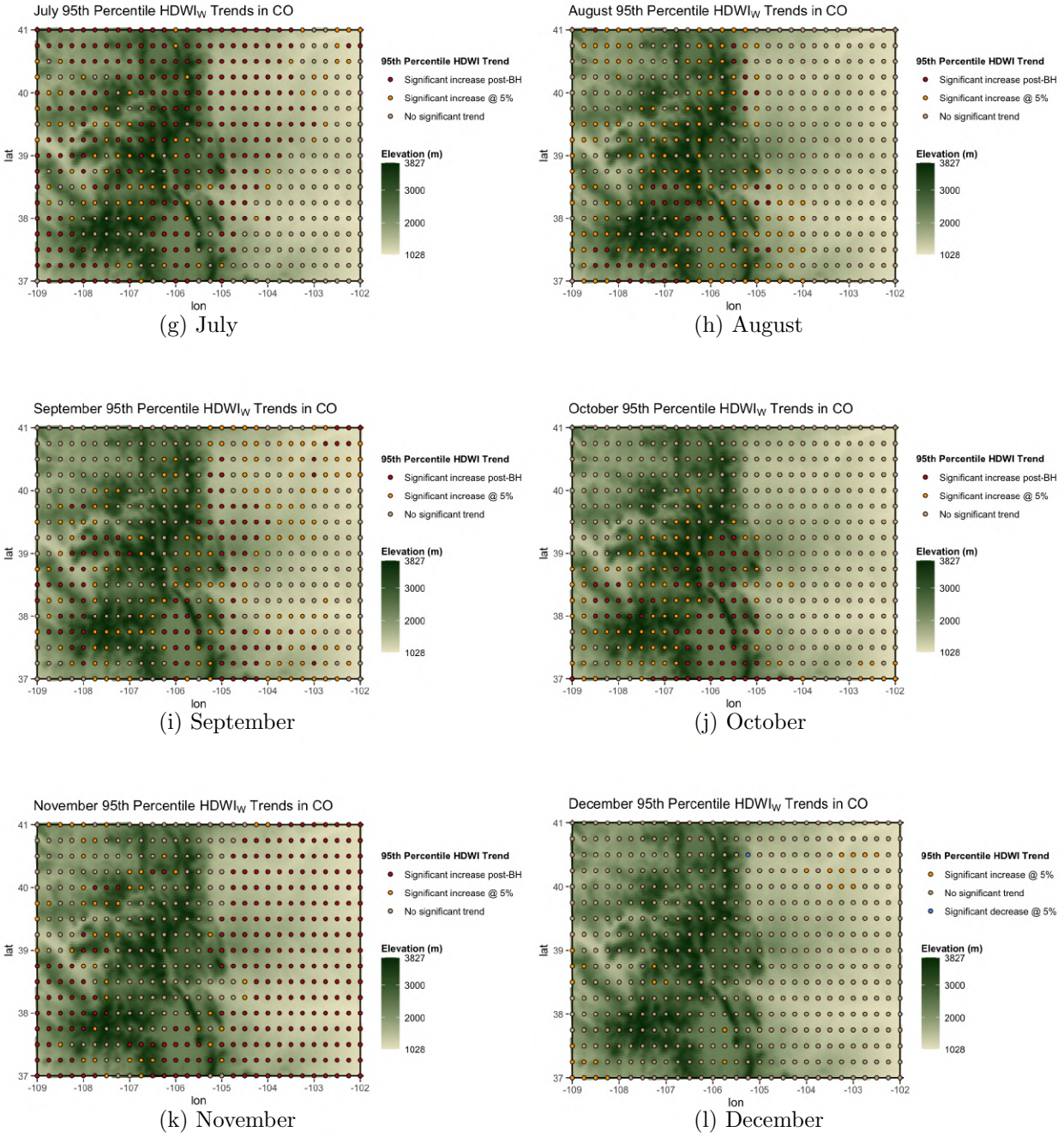

(g) July (h) August

(i) September (j) October

(k) November (l) December

Figure F.2: 95th percentile $HDWI_W$ test results for trends across all of Colorado.